Published in final edited form as:
Nat Immunol. 2016 March ; 17(3): 331–343. doi:10.1038/ni.3349.

Multifunctional role of the transcription factor Blimp1 in coordinating plasma cell differentiation

Martina Minnich[1], **Hiromi Tagoh**[1], **Peter Bönelt**[1], **Elin Axelsson**[1,5], **Maria Fischer**[1], **Beatriz Cebolla**[1], **Alexander Tarakhovsky**[2], **Stephen L. Nutt**[3,4], **Markus Jaritz**[1], and **Meinrad Busslinger**[1,#]

[1]Research Institute of Molecular Pathology (IMP), Vienna Biocenter (VBC), Dr. Bohr-Gasse 7, A-1030 Vienna, Austria

[2]Laboratory of Lymphocyte Signaling. The Rockefeller University, New York, USA

[3]The Walter and Eliza Hall Institute of Medical Research, Parkville, Victoria, Australia

[4]Department of Medical Biology, The University of Melbourne, Parkville, Victoria, Australia

Abstract

Blimp1 is an essential regulator of plasma cells. Here we studied its functions in plasmablast differentiation by identifying regulated Blimp1 target genes. Blimp1 promoted plasmablast migration and adhesion. It repressed several transcription factor genes and *Aicda*, thus silencing B-cell-specific gene expression, antigen presentation and class switch recombination in plasmablasts. It directly activated genes, leading to increased expression of the plasma cell regulator IRF4 and proteins involved in immunoglobulin secretion. Blimp1 induced immunoglobulin gene transcription by controlling *Igh* and *Igk* 3' enhancers and regulated the posttranscriptional expression switch from the membrane-bound to secreted immunoglobulin heavy-chain by activating *Ell2*. Notably, Blimp1 recruited chromatin-remodeling and histone-modifying complexes to regulate its target genes. Hence, many essential functions of plasma cells are under Blimp1 control.

[#]To whom correspondence should be addressed: phone: (+43/1) 797 30 – 3150 fax: (+43/1) 797 30 – 223150 busslinger@imp.ac.at.
[5]Present address: Gregor Mendel Institute of Molecular Plant Biology, Austrian Academy of Sciences, Dr. Bohr-Gasse 3, A-1030 Vienna, Austria

Author Contributions

M.M. did most experiments; H.T. performed the ATAC-seq, IRF4 ChIP-seq, EMSA and Blimp1-ER induction experiments; P.B. performed the migration, adhesion and HEK-293T co-precipitation experiments; B.C. generated the targeted *Prdm1*$^{ihCd2\text{-}neo}$ ES cells; E.A. and M.J. did the bioinformatic analysis of all RNA-seq and ChIP-seq data, respectively; M.F. performed the bioinformatics analysis of the immunoglobulin gene transcripts; A.T. and S.N. provided advice and important mouse strains; M.M., H.T. and M.B. planned the project, designed the experiments and wrote the manuscript.

Competing financial interests

The authors declare no competing financial interests.

Accession numbers

The RNA-seq, ChIP-seq and ATAC-seq data are available at the Gene Expression Omnibus (GEO) repository under the accession numbers GSE71698.

Europe PMC Funders Author Manuscripts

Keywords

Blimp1; gene activation and repression; transcriptional network; cell adhesion and migration; immunoglobulin gene control; chromatin regulation; epigenetic regulators

Introduction

Plasma cells play an important role in the acute response to infection and in long-term protection of the host by providing humoral immunity through continuous secretion of antibodies1. Activation of B-cells by antigen leads to differentiation of short-lived, antibody-secreting plasmablasts, which develop into quiescent long-lived plasma cells upon migration to survival niches in the bone marrow1. Plasmablast formation is associated with marked changes in cell morphology and gene expression1,2. The rearranged immunoglobulin heavy-chain (*Igh*) gene switches expression from its B-cell-specific mRNA encoding the membrane-bound protein to the plasma-cell-specific transcript encoding the secreted Ig heavy chain1. Moreover, the expression of the *Igh* and immunoglobulin light-chain (*Igk*, *Igl*) genes is strongly increased in plasmablasts, resulting in the secretion of large amounts of immunoglobulin proteins1,2. To cope with this output, antibody-secreting cells greatly increase their secretory machinery by expanding the endoplasmic reticulum (ER). These changes are a consequence of the unfolded protein response (UPR) that is induced by protein overloading of the ER and restores the folding, processing and export of proteins passing through the ER. The transcription factor XBP1, which is activated by the UPR3, is a central regulator of the UPR gene expression program4 and, as a consequence, is essential for immunoglobulin secretion of plasma cells5.

While plasmablasts are generated in the absence of XBP16, their differentiation depends on the transcription factors IRF4 (ref. 7) and Blimp1 (ref. 8). IRF4 initiates plasmablast differentiation by activating the *Prdm1* gene (encoding Blimp1)9,10. The B-lymphocyte-induced maturation protein 1 (Blimp1)11 is a Krüppel-type zinc finger protein12 that is able to induce plasmacytic differentiation upon ectopic expression in mature B-cells12. Within the B-lymphoid lineage, Blimp1 is exclusively expressed in antibody-secreting cells13, which are lost in mice with B-cell-specific deletion of *Prdm1*, demonstrating that Blimp1 is essential for plasma cell generation8. Blimp1 is, however, not required for the initiation of plasmablast formation, as its loss arrests differentiation at the pre-plasmablast stage14.

Blimp1 is a transcriptional repressor that silences the B-cell gene expression program in plasma cells15. Consistent with this notion, Blimp1 interacts with co-repressors such as the H3K4 demethylase LSD1 (ref. 16), H3K9 methyltransferase G9a17, Groucho family proteins18 and histone deacetylases19. To date, only five genes coding for the transcription factors c-Myc20, Pax5 (ref. 21), CIITA15,22, SpiB15 and Id3 (ref. 15) are considered to be directly repressed by Blimp1. All Blimp1-dependent gene expression changes were so far identified by gain-of-function experiments in human and mouse B-cell lines that ectopically expressed Blimp115,23. However, these experiments could not distinguish between direct and indirect effects of Blimp1 activity and were furthermore performed in B-cells rather than

plasmablasts15,23. Hence, little is known to date about the molecular mechanisms, by which Blimp1 controls plasma cell differentiation.

Here we have comprehensively analyzed the molecular role of Blimp1 at the onset of plasmablast differentiation, which revealed that Blimp1 directly controls many essential functions of plasmablasts and plasma cells.

Results

Blimp1 controls a large part of the gene expression changes associated with plasma cell differentiation

To study the molecular function of Blimp1, we first defined the gene expression changes occurring during differentiation of activated B-cells to plasmablasts. Upon LPS stimulation for 4 days, $B220^+$ B-cells from spleen and lymph nodes of *Prdm1*$^{Gfp/+}$ mice13 differentiated into activated B-cells ($CD138^-GFP^-CD22^+CXCR4^-$), immunoglobulin-secreting pre-plasmablasts ($CD138^-GFP^+CD22^-CXCR4^+$) and plasmablasts ($CD138^+GFP^+CD22^-CXCR4^+$)14 (Fig. 1a; Supplementary Fig. 1a), which were analyzed by RNA-sequencing. Differentially expressed genes were identified in all RNA-seq comparisons, if they revealed an expression difference of > 3-fold, an adjusted *P* value of < 0.1 and an RPKM value of > 3 in one of the two cell populations. Thus, 648 genes were up-regulated and 424 genes were down-regulated in the B-cell-to-plasmablast transition (Fig. 1b; Supplementary Table 1). Most regulated genes were similarly expressed in pre-plasmablasts compared to plasmablasts (Supplementary Fig. 1b). RNA-seq comparison of quiescent plasma cells from the bone marrow with non-proliferating mature B-cells from lymph nodes (Supplementary Fig. 1c) identified 1260 up-regulated and 900 down-regulated genes in plasma cells compared to follicular B-cells (Fig. 1c; Supplementary Table 2). Importantly, 474 (73%) of the up-regulated genes and 274 (65%) of the down-regulated genes in in vitro differentiated plasmablasts were similarly regulated in plasma cells in vivo (Fig. 1d).

To determine the Blimp1-dependent part of the plasmablast expression signature, we used the *Cd23*-Cre line24 to delete the floxed *Prdm1* allele25 in B-cells of *Cd23*-Cre *Prdm1*$^{Gfp/fl}$ mice, which additionally carried the *Prdm1*^{Gfp} null allele13. LPS-induced differentiation of *Cd23*-Cre *Prdm1*$^{Gfp/fl}$ B-cells for 4 days gave rise to all three cell types (Fig. 1e), although the small plasmablast population still retained the intact floxed *Prdm1* allele (Fig. 1f), consistent with a stringent requirement of Blimp1 for plasmablast formation8,14. As pre-plasmablasts consisted of cells containing the intact floxed (fl) or deleted (Δ) *Prdm1* allele (Fig. 1f), we used CD22 expression, which is repressed by Blimp1 (Fig. 1a,e), to fractionate the cell mixture into *Prdm1*-deleted (*Prdm1*$^{Gfp/\Delta}$) $CD22^+CD138^-GFP^+$ pre-plasmablasts and *Prdm1*-expressing (*Prdm1*$^{Gfp/fl}$) $CD22^-CD138^-GFP^+$ pre-plasmablasts (Fig. 1f; Supplementary Fig. 1d). RNA-seq comparison of *Prdm1*$^{Gfp/\Delta}$ and control *Prdm1*$^{Gfp/+}$ pre-plasmablasts identified 278 Blimp1-activated and 257 Blimp1-repressed genes in pre-plasmablasts (Fig. 1g Supplementary Table 3). As 245 genes were also up-regulated and 173 genes were down-regulated during the B-cell-to-plasmablast transition (Fig. 1b), they were regarded as relevant Blimp1-regulated genes (Fig. 1h). Hence, Blimp1 activated 38% (245) of all up-regulated genes (648) and repressed 41% (173) of all down-regulated genes (424) during plasmablast differentiation. To visualize some gene expression patterns, we focused

on cell surface receptor genes, indicating that 12 genes (*Alcam*, *Ccrl2*, *Crlf1*, *Dll3*, *Epcam*, *Il6st*, *Itgb5*, *Lag3*, *H13*, *Tigit*, *Tmem66*, *Tspan13*) were significantly activated and 16 genes (*Ccr7*, *Cd22*, *Cd37*, *Cd72*, *Faim3*, *Ffar1*, *Lilrb3*, *Il10ra*, *Il9r*, *Ly86*, *Notch2*, *Pecam1*, *Sell*, *Siglecg*, *Tlr1*, *Tlr9*) were strongly repressed by Blimp1 in plasmablasts (Fig. 1i; Supplementary Fig. 1e; data not shown). Hence, terminal B-cell differentiation leads to a major, Blimp1-dependent change in expression and thus signaling of cell surface receptors.

Blimp1-dependent genes were similarly expressed in Blimp1-negative (GFP^-) activated B-cells ($Prdm1^{Gfp/+}$) and Blimp1-deficient (GFP^+) pre-plasmablasts ($Prdm1^{Gfp/\Delta}$) (Fig. 1i; Supplementary Fig. 1e), suggesting that Blimp1 loss may arrest differentiation at the activated B-cell stage. However, 77 genes were normally activated or repressed during the B-cell-to-pre-plasmablast transition in the absence of Blimp1, as exemplified by the activated genes *Rgs10*, *Socs2*, *Top1*, *Tubb6*, *Slamf7* and *Cdkn2b* and repressed genes *Bach2*, *Ccr6*, *Il12a* and *Irf8* (Fig. 1j; Supplementary Fig. 1f). Hence, the loss of Blimp1 blocks differentiation at a pre-plasmablast stage as published14.

Identification of regulated Blimp1 target genes

To determine Blimp1 binding, we generated a $Prdm1^{Bio}$ allele by inserting a C-terminal biotin acceptor sequence (Bio) at the last codon of Blimp1 (Supplementary Fig. 2a,b), which was efficiently biotinylated by the *E. coli* biotin ligase BirA in LPS-stimulated $Prdm1^{Bio/Bio}$ $Rosa26^{BirA/+}$ plasmablasts, thus facilitating streptavidin-mediated pulldown of Blimp1-Bio (Supplementary Fig. 2c). Importantly, $Prdm1^{Bio/Bio}$ $Rosa26^{BirA/BirA}$ mice gave rise to normal B-cell development and immune responses at day 14 after NP-KLH immunization (Supplementary Fig. 2d-f), indicating that the C-terminal insertion did not affect Blimp1 function. LPS-induced $CD138^+$ plasmablasts of the $Prdm1^{Bio/Bio}$ $Rosa26^{BirA/BirA}$ genotype were next analyzed by Bio-ChIP-sequencing26 (Fig. 2a). Peak calling with a stringent P value of $< 10^{-10}$ determined 8,742 Blimp1-binding regions, which defined 4,899 Blimp1 target genes in plasmablasts (Fig. 2b). Analysis of the Blimp1 peak sequences with de novo motif discovery programs identified a Blimp1-binding motif (Fig. 2c), that resembles the published Blimp1 recognition sequence27 and was found at a high frequency (70%) at Blimp1 peaks in plasmablasts (Fig. 2c). By determining the overlap between the Blimp1-bound genes (Fig. 2b) and Blimp1-regulated genes (Fig. 1h), we identified 93 potentially directly activated and 121 potentially directly repressed Blimp1 target genes that were regulated more than 3-fold by Blimp1 in pre-plasmablasts (Fig. 2d; Supplementary Table 4). RNA expression and Blimp1 binding are shown for *Aicda* as a repressed target and for *Il10*, *Mzb1*, *Hspa5* (BiP) and *Ssr2* as activated targets (Fig. 2e; Supplementary Fig. 2g).

These data suggested a novel function for Blimp1 as a transcriptional activator in addition to its known role in gene repression11,15. To investigate whether Blimp1 directly activates gene transcription, we generated a posttranslational induction system by fusing the full-length Blimp1 protein at its C-terminus to the ligand-binding domain of a mutant estrogen receptor (ER^{T2}) that interacts only with the estrogen analogue 4-hydroxytamoxifen (OHT)28. We infected the B-cell line WEHI-231 with a MiCD2-Blimp1-ER^{T2} retrovirus and selected single-cell clones that efficiently repressed the Blimp1 target gene *Cd22* upon OHT treatment (Supplementary Fig. 2h). OHT addition to the WEHI-Blimp1-ER^{T2} cells for

6 hours led to a 2-4-fold increased transcription of 14 activated target genes as revealed by RT-qPCR analysis of nascent transcripts (Fig. 2f). As the Blimp1-ER^{T2} protein is constitutively expressed in an inactive form in WEHI-Blimp1-ER^{T2} cells, it can be activated by OHT addition even in the presence of the translation inhibitor cycloheximide (CHX), which prevents indirect transcriptional effects. Under these conditions, the Blimp1-ER^{T2} protein could still induce transcription of all 14 genes within 6 hours of OHT treatment (Fig. 2f). As shown by ChIP-qPCR analysis, the active histone mark H3K4me2 was induced in WEHI-Blimp1-ER^{T2} cells already at 2 hours, and H3K27ac was increased at 2 or 6 hours after OHT addition at Blimp1-binding sites of 4 activated target genes (Fig. 2g). Hence, the Blimp1-ER^{T2} induction system provided clear evidence that Blimp1 can directly activate its target genes at the transcription and chromatin level. Notably, the Blimp1-binding sites at repressed target genes rapidly lost H3K27ac within 2 hours and gained the repressive H3K27me3 modification with a delay at 6 to 12 hours after OHT induction of Blimp1 activity (Fig. 2h), indicating that histone deactylation precedes H3K27 methylation at repressed target genes.

Functions of proteins encoded by Blimp1 target genes

The regulated Blimp1 target genes code for proteins of distinct functional classes (Fig. 3a; Supplementary Table 4). Half of all repressed Blimp1 target genes code for 32 (26%) signal transducers, 16 (13%) cell surface receptors and 13 (11%) transcriptional regulators, indicating that Blimp1 suppresses B-cell signaling in plasmablasts (Fig. 3a). Consequently, Blimp1 interferes with B-cell and Toll-like receptor signaling, antigen presentation and T-cell co-stimulation, class switch recombination and somatic hypermutation as well as cell adhesion and migration (Fig. 3a; Supplementary Fig. 3). Blimp1 activated fewer genes coding for 15 (16%) signal transducers, 7 (7.5%) cell surface receptors and 7 (7.5%) transcriptional regulators (Fig. 3a). Importantly, we identified 9 activated and 21 repressed target genes coding for cell surface proteins, signal transducers and cytoskeletal proteins involved in cell adhesion and migration (Fig. 3a; Supplementary Fig. 3), suggesting that Blimp1 controls the migratory and sessile behavior of plasmablasts29,30. In transwell migration assays, control pre-plasmablasts (*Prdm1*$^{Gfp/+}$) migrated faster than activated B-cells towards the chemokine CXCL12 (Fig. 3b). This increased migration was, however, not observed for Blimp1-deficient pre-plasmablasts (*Prdm1*$^{Gfp/\Delta}$), although *Cxcr4* (encoding the receptor for CXCL12) was similarly expressed in pre-plasmablasts of both genotypes (data not shown). In the presence of CXCL12, the control pre-plasmablasts also adhered better than Blimp1-deficient pre-plasmablasts to surfaces coated with ICAM-1 or VCAM-1 (Fig. 3c). Hence, Blimp1 increases both the migration and substrate adhesion of plasmablasts. In addition, plasmablasts communicate with their environment by secreting VEGF-A, Wnt10a and IL-10, as shown by Blimp1-activated expression of these genes (Fig. 2e; Supplementary Fig. 3). Plasmablasts also express, in a Blimp1-dependent manner, the genes *Tigit*, *Clta4*, *Tmem66* and *Lag3*, coding for inhibitory cell surface receptors with known functions in T cells (Fig. 3; Supplementary Fig. 3).

Notably, 78 Blimp1-activated genes code for proteins implicated in ER stress control and immunoglobulin secretion (data not shown). Blimp1 binding was absent at 58 of these genes, which are likely controlled by the UPR regulator XBP1. Importantly, Blimp1 bound

to and activated 20 genes coding for proteins implicated in ER function and ER stress control in plasmablasts (Fig. 3; Supplementary Fig. 3). Moreover, Blimp1 directly activated five (*Derl1*, *Mzb1*, *Ssr2*, *Tram2*, *Cnst*) of these genes in WEHI-Blimp1-ER^{T2} cells (Fig. 2f). Hence, Blimp1, in addition to XBP1, directly contributes to the regulation of immunoglobulin secretion.

Blimp1-dependent transcriptional network in plasmablasts

IRF4, another essential plasma cell transcription factor7, binds with the Ets protein PU.1 to the Ets-IRF composite element (EICE)31, which resembles the Blimp1 motif (Fig. 2c), suggesting that IRF4 and Blimp1 can bind the same recognition sequence. To test this hypothesis, we determined the binding of IRF4 and PU.1 in plasmablasts by ChIP-seq analysis (Fig. 4a), which identified 19,735 and 39,772 IRF4 and PU.1 peaks, respectively. Colocalization of PU.1, IRF4 and Blimp1 peaks (Supplementary Fig. 4a) revealed that most Blimp1-binding regions in the genome (45%) and at regulated target genes (52%) overlapped with PU.1 and IRF4 peaks (Fig. 4b). Sorting of a heat map containing all 3,806 common peaks according to the IRF4 peak density demonstrated that the PU.1- and IRF4-binding densities largely correlated with each other consistent with the presence of the EICE motif (Supplementary Fig. 4a,b). However, sorting for the Blimp1-binding density revealed no correlation with IRF4 and PU.1 peaks in agreement with the discovery of the Blimp1 motif in the common peaks (Supplementary Fig. 4a,b), suggesting that Blimp1 binding is independent of PU.1 and IRF4 binding. However, the Blimp1 and EICE motifs were often co-localized at the same position, which contained a common binding motif deviating at several positions from the Blimp1 and EICE motifs (Fig 4c). Electrophoretic mobility shift assay demonstrated that Blimp1 and the PU.1/IRF4 complex could bind to the common binding motif present at the repressed target genes *Vrk2* (Fig. 4d; intron 2) and *Tlr9* (intron 1; data not shown). Addition of an anti-V5 antibody retarded only the migration of the Blimp1-Bio (V5) complex, whereas anti-PU.1 and anti-IRF4 antibodies only affected their respective complexes (Fig. 4d). Hence, Blimp1 and the PU.1/IRF4 complex can bind to the same sequence motif, although in a mutually exclusive manner. Consequently, ChIP-qPCR experiments demonstrated that OHT-induced Blimp1 activity in WEHI-Blimp1-ER^{T2} could displace IRF4 and PU.1 at common binding sites of the *Tlr9*, *Vrk* and *Aff3* genes in contrast to the unaffected IRF4 and PU.1 binding at the EICE elements of *Cobll1* and *Rps* that were not bound by Blimp1-ER (Fig. 4e; Supplementary Fig. 4c).

Blimp1 activated 7 and repressed 13 transcription factor genes (Fig. 5a,b), which contained one or multiple Blimp1-binding sites in plasmablasts, consistent with direct regulation by Blimp1 (Supplementary Fig. 5a,b). Our analysis revealed the entire Blimp1-binding pattern for *Ciita*22, *Id3* (ref. 15), *Pax5* (ref. 15,21) and *Spib*15 (Supplementary Fig. 5a), which were previously considered to be silenced by Blimp1. The other 9 Blimp1-repressed transcription factor genes were not previously associated with Blimp1 regulation and encode a co-repressor (Tle3), transcription elongation factor (Aff3), three transcription factors (Dek, Irf2bp2, Zeb2) with unknown B-cell functions and the four regulators Bcl11a32, Gfi1b33, Hhex34 and Klf2 (ref. 35), which control important aspects of B-cell development. Notably, *Bcl6* coding for an essential regulator of germinal center B-cells contained several Blimp1-binding sites (Supplementary Fig. 5c), consistent with its known Blimp1-dependent

repression15, although we failed to identify *Bcl6* as a Blimp1-repressed gene due to its low expression in activated B-cells (Fig. 5c).

Of the 7 Blimp1-activated transcription factor genes, only *Irf4* and *Ell2* have known roles in plasma cell differentiation7,9 or immunoglobulin secretion36–38, respectively. Moreover, the activated target gene *Eaf2* codes for a positive regulator of the transcription elongation activity of Ell2 (ref. 39).

Blimp1-dependent activation of immunoglobulin gene transcription in plasmablasts

XBP1, an essential regulator of the UPR gene expression program4,5, acts downstream of Blimp1 in the regulatory cascade of terminal B-cell differentiation4,6. Our RNA-seq data combined with RT-qPCR analysis of nascent transcripts demonstrated an essential role for Blimp1 in the strong up-regulation of *Xbp1* transcription in pre-plasmablasts compared to activated B-cells (Fig. 5d,e). However, the *Xbp1* locus was devoid of Blimp1-binding sites in a region spanning from +147 kb upstream to -219 kb downstream of the gene (Supplementary Fig. 5d), suggesting that *Xbp1* is indirectly activated by Blimp1. RNA-seq analysis furthermore revealed a strong increase in *Igh* and *Igk* mRNA expression in control pre-plasmablasts (20x, *Igh*; 13x, *Igk*) and plasmablasts (29x, *Igh*; 18x, *Igk*) compared to activated B-cells (Fig. 6a,b; Supplementary Fig. 6a). This strong mRNA increase is caused by transcriptional activation, as a similarly robust up-regulation of nascent *Igh* and *Igk* transcripts was observed by RT-qPCR analysis (Fig. 6c). Consequently, the mRNAs encoding the secreted $Ig\mu_s$, $Ig\gamma 2b_s$ and $Ig\gamma 3_s$ proteins were strongly increased during terminal B-cell differentiation in contrast to the constant expression of the mRNA encoding the membrane-bound $Ig\mu_m$ protein (Fig. 6d,e). In the absence of Blimp1, the *Igh* and *Igk* mRNAs and nascent transcripts were only minimally increased (Fig. 6a-c) and the switch to $Ig\mu_s$, $Ig\gamma 2b_s$ and $Ig\gamma 3_s$ transcripts did not take place in Blimp1-deficient pre-plasmablasts (Fig. 6d,e). Hence, Blimp1 is involved in the strong up-regulation of *Igh* and *Igk* transcription as well as in the posttranscriptional switch to the *Igh* mRNA isoforms encoding the secreted Ig heavy-chain in plasmablasts.

High expression of the *Igh* gene in plasma cells depends on the 3' regulatory region (3'RR) consisting of four enhancers (HS1/2, HS3A, HS3B and HS4) at the 3' end of the *Igh* locus40. Mapping of open chromatin regions (known as DNase I hypersensitive [DHS] sites) by ATAC-seq41 revealed that all four enhancers were already present in open chromatin in activated B-cells (Fig. 6f). In contrast, the accessibility at HS3A and HS3B was strongly reduced in Blimp1-deficient pre-plasmablasts, although the density at all genomic DHS sites was similar in these cells compared to control pre-plasmablasts and plasmablasts (Supplementary Fig. 6c,d). Blimp1 bound only to the HS1/2 enhancer, whereas IRF4 interacted with all four enhancers and PU.1 only with HS4 in the 3'RR (Fig. 6f). These data therefore indicate that Blimp1 is indirectly responsible for maintaining open chromatin at the 3'RR in plasmablasts. The loss of Blimp1 also resulted in reduced chromatin accessibility of all enhancers at the 3' end of the *Igk* locus in pre-plasmablasts, although Blimp1 bound only weakly to the iE_κ enhancer and a novel plasmablast-specific DHS site (Supplementary Fig. 6b).

Chromatin changes at regulated Blimp1 target genes in plasmablasts

In addition to DHS sites, we mapped active (H3K4me2, H3K4me3, H3K9ac) and repressive (H3K27me3) histone marks by ChIP-seq in *Prdm1*$^{Gfp/+}$ activated B-cells and plasmablasts at day 4 of LPS stimulation (Supplementary Fig. 7a,b). We defined 'active' promoters by the presence of a DHS site at an annotated transcription start site (TSS) and 'active' distal elements (potential enhancers) by the presence of a DHS site in the absence of a TSS. In plasmablasts, 15.4% (1,349) of all Blimp1-binding sites (8,742) were located at 'active' promoters (+DHS +TSS), which were embedded in active (86%) or bivalent (14%) chromatin (Fig. 7a; Supplementary Fig. 7b). Half (4,201; 48%%) of all Blimp1 peaks mapped to 'active' distal elements (+DHS -TSS), which carried active (56%), poised (11%) or bivalent (26%) chromatin (Fig. 7a). Hence, Blimp1 primarily binds to active promoters and distal elements in plasmablasts. Notably, many Blimp1 peaks (3,265; 37.3%) were also located at less accessible genomic regions (-DHS -TSS) (Fig. 7a; Supplementary Fig. 7b).

The histone modifications analyzed did not change during the B-cell-to-plasmablast transition at Blimp1-binding sites of genes that were not regulated by Blimp1, as shown by heat maps and density diagrams (Fig. 7b-d). The abundance of all three active histone marks was, however, increased at Blimp1-binding sites of activated target genes in plasmablasts compared to activated B-cells (Fig. 7b,d). In contrast, the three active chromatin modifications were reduced at Blimp1-binding sites of repressed target genes in plasmablasts relative to activated B-cells (Fig. 7c,d). Notably, the repressive H3K27me3 modification was only present in plasmablasts at Blimp1-binding sites of repressed target genes, where it spread in both directions (Fig. 7c,d,f). No difference in H3K27me3 abundance was observed at DHS sites of repressed genes lacking Blimp1-binding sites (Supplementary Fig. 7c). Importantly, ChIP-seq analysis of pre-plasmablasts revealed that H3K27me3 was absent at the Blimp1-binding sites of repressed target genes in Blimp1-deficient pre-plasmablasts in contrast to control pre-plasmablasts (Fig. 7e,f; Supplementary Fig. 7d). These data suggest that Blimp1 is involved in recruiting the H3K27-methylating Polycomb repressive complex 2 (PRC2)42 to its repressed target genes in plasmablasts. The prevailing model predicts, however, that the recruitment of Polycomb complexes to DNA occurs by default at CpG islands (CGI) lacking active chromatin rather than by DNA-binding proteins43. Contrary to this model, CpG islands, which were mapped by CAP-seq in mouse blood cells44, were not enriched at Blimp1-binding sites of repressed target genes in contrast to their presence at Blimp1-binding sites of non-regulated and activated target genes (Fig. 7b-d). Moreover, CpG islands were also not enriched at the Blimp1-binding sites displaying bilateral H3K27me3 spreading (Supplementary Fig. 7e). Blimp1-dependent spreading of H3K27me3 in the absence of a CpG island is shown for a Blimp1-binding site in intron 6 of *Pax5* (Fig. 7f) and intron 2 of *Vrk2* (Supplementary Fig. 7f), which furthermore demonstrated that other Blimp1-binding sites at these repressed genes were not associated with H3K27me3^{+} chromatin. Hence, Blimp1 binding can induce, in a context-dependent but CpG island-independent manner, the spreading of H3K27me3 at repressed target genes in plasmablasts.

Blimp1 recruits chromatin modifiers and remodelers to regulate its target genes.

To investigate a possible interaction of Blimp1 with PRC2, we performed streptavidin pulldown experiments with nuclear extracts of LPS-stimulated *Prdm1*$^{Bio/Bio}$ *Rosa26*$^{BirA/+}$ and control *Prdm1*$^{+/+}$ *Rosa26*$^{BirA/+}$ plasmablasts. Ezh2, the catalytic subunit of PRC2 (ref. 42), was specifically co-precipitated with the biotinylated Blimp1-Bio protein (Fig. 8a). We verified this interaction in HEK-293T cells that were transiently transfected with expression vectors encoding Blimp1-Bio-IRES-BirA and Myc-tagged Ezh2 or IRF4 proteins. Streptavidin pulldown of nuclear extracts revealed that Myc-Ezh2 was specifically co-precipitated with the biotinylated V5-tagged Blimp1-Bio protein in contrast to Myc-IRF4 (Fig. 8b). In the reverse order, Blimp1-Bio was pulled down with Myc-Ezh2 (Fig. 8c) by co-immunoprecipitation with an anti-Myc antibody. We next studied the role of PRC2 in Blimp1-mediated gene repression by adding the Ezh2 small molecular inhibitor GSK343 to *Prdm1*$^{Gfp/+}$ B-cells at the start of LPS-induced plasmablast differentiation. RNA-sequencing of GSK343- and control DMSO-treated pre-plasmablasts demonstrated that many repressed Blimp1 target genes were partially silenced upon Ezh2 inhibition, which prevented H3K27 methylation (Supplementary Fig. 8a,b). The observed incomplete repression is consistent with a role of PRC2 in maintaining the silenced expression state that is initially brought about by histone deacetylases and demethylases42 (Fig. 2h).

Mass-spectrometric identification of proteins that were precipitated by streptavidin pulldown from nuclear extracts of *Prdm1*$^{Bio/Bio}$ *Rosa26*$^{BirA/+}$ plasmablasts revealed 9 components of the chromatin-remodeling BAF complex45 (BAF45D, 47, 53A, 57, 60A, 60B, 155, 170, Brg1), 3 subunits of the nucleosome-remodeling NuRD complex45 (GATAD2A, MTA1, CHD4), 3 proteins of the NCoR complex46 (TBL1, TBLR1, NCOR1) and 2 factors of the SIN3 co-repressor complex46 (SAP18, SIN3A) (data not shown). We confirmed these interactions by co-precipitating Blimp1-Bio from plasmablast extracts with Brg1 (BAF), CHD4 (Mi-2β; NuRD), MBD3 (NuRD), SIN3A and histone deacetylase 1 (HDAC1), which is a component of the NuRD, NCoR and SIN3 complexes46 (Fig. 8d). Hence, Blimp1 can interact, in addition to PRC2, with the chromatin-remodeling BAF and NuRD complexes as well as the histone-deacetylating NCoR and SIN3 co-repressor complexes.

The Blimp1-ER induction system is ideal for studying the recruitment of Blimp1-interacting complexes to Blimp1 target genes as the ligand OHT prevents the binding of co-regulators to the ER ligand-binding domain by inducing an inactive conformation47. We thus stimulated WEHI-Blimp1-ER^{T2} with OHT for a short time (up to 2h) followed by ChIP-qPCR analysis with antibodies detecting specific subunits of the Blimp1-interacting complexes (Fig. 8e,f). Within 30 minutes of OHT treatment, the Blimp1-ER^{T2} protein interacted with its binding sites at repressed and activated Blimp1 target genes (Fig. 8e,f). However, it could not bind to the control *Cd19* promoter and thus failed to recruit the HDAC1, Ezh2, CHD4, NCOR1 and Brg1 proteins to the *Cd19* gene (Supplementary Fig. 8c). In contrast, HDAC1 started to accumulate, within 1 hour of OHT addition, at the Blimp1-binding sites of the repressed target genes *Spib*, *Aff3* and *Kynu* in contrast to the *Tlr9* and *Il10ra* gene (Fig. 8e). The Brg1, CHD4 and NCOR1 proteins were recruited within 1 hour and Ezh2 within 2 hours of OHT treatment to the Blimp-binding sites of all 5 repressed target genes (Fig. 8e). As the BAF complex can function both as a co-activator or co-repressor45, Blimp1 could recruit this

complex, but not HDAC1, to its binding sites at the activated target genes *Gnaz*, *Pik3cg* and *Tram2* (Fig. 8f). Hence, Blimp1 recruits chromatin-remodeling (BAF, NuRD) and chromatin-modifying (NCoR, NuRD, PRC2) complexes to regulate its target genes in plasmablasts.

Discussion

Blimp1 is an essential regulator of plasma cell development11, and yet little is known about its molecular functions in terminal B-cell differentiation. Previous attempts to identify Blimp1-regulated genes largely failed because of their experimental design, as differential gene expression was analyzed in mature B-cell lines ectopically expressing Blimp1 activity rather than in plasmablasts15,23. Here we compared Blimp1-deficient and control pre-plasmablasts by RNA-sequencing, demonstrating that Blimp1 controls a large part (~40%) of the gene expression changes occurring during the B-cell-to-plasmablast transition. Notably, several genes, which are activated or repressed during this developmental transition, are normally regulated in Blimp1-deficient pre-plasmablasts, providing molecular evidence that Blimp1 loss blocks differentiation at a pre-plasmablast stage14. By combining Blimp1-mediated regulation with Blimp1-binding, we identified 93 activated and 121 repressed Blimp1 target genes, which provided novel insight into the molecular functions of Blimp1 in controlling plasma cell differentiation.

Blimp1 is considered to be a dedicated transcriptional repressor11, and yet our analysis identified 93 activated Blimp1 target genes. Here we provided several lines of evidence that Blimp1 can function as a transcriptional activator. First, stimulation of Blimp1 activity in WEHI-Blimp1-ER^{T2} B-cells rapidly induced the transcription of activated Blimp1 target genes even upon protein synthesis inhibition, which prevented indirect activation. Second, two hours of Blimp1 activation were sufficient to increase active histone modifications at Blimp1-binding sites of activated target genes in WEHI-Blimp1-ER^{T2} B-cells. Third, active histone marks were also increased at Blimp1-binding sites of activated target genes in plasmablasts compared to activated B-cells. Fourth, Blimp1 interacted in plasmablasts with the chromatin-remodeling BAF complex that functions as a transcriptional co-activator45. Finally, Blimp1 recruited the BAF complex to binding sites at activated target genes within one hour of OHT treatment in WEHI-Blimp1-ER^{T2} B-cells. Notably, an important class of activated Blimp1 target genes codes for proteins involved in ER function and protein secretion. Hence, Blimp1, in addition to XBP1, contributes to the regulation of the UPR in plasmablasts and plasma cells.

Whereas previous analyses of Blimp1's role in the control of immunoglobulin secretion yielded conflicting results8,14, our study revealed an essential role for Blimp1 in the control of the posttranscriptional switch from the membrane-bound to secreted Ig heavy-chain protein. This Blimp1-dependent switch is likely explained by up-regulation of the activated Blimp1 target genes *Ell2* and *Eaf2* in plasmablasts. ELL2 together with its partner protein EAF2 increases the transcription elongation rate of RNA polymerase II (ref. 39). In the context of *Igh* gene expression, ELL2 promotes the generation of transcripts encoding the secreted Ig heavy-chain protein by changing the alternative processing at their 3' end[36-38]. The membrane-encoding or secreted *Igh* mRNAs are generated by the mutually exclusive

use of a splice site versus a cleavage/polyadenylation site at the 3' end of the *Igh* pre-mRNA transcript, respectively. ELL2 tilts the balance towards the generation of the secreted *Igh* mRNA by promoting the skipping of the splice site and enhancing the use of the promoter-proximal polyadenylation site36. Notably, Blimp1 also contributes to the biosynthesis and polymerization of secreted IgM proteins in the ER by activating the expression of the hexameric lectin LMAN1 (ref. 48) and the two interacting, ER-resident chaperones HSP90B1 and MZB1 (ref. 49).

In addition to controlling *Igh* mRNA processing, Blimp1 strongly activates *Igh* and *Igk* gene transcription during the B-cell-to-plasmablast transition. All four enhancer in the 3'RR of the *Igh* locus have been implicated in the strong up-regulation of *Igh* transcription in plasmablasts40, and, consistent with this notion, the loss of Blimp1 reduces the chromatin accessibility at two of these enhancers (HS3A, HS3B) in pre-plasmablasts. However, Blimp1 binds only to the HS1/2 enhancer, which is dispensable for high Ig secretion50, suggesting that Blimp1 indirectly regulates the activity of the 3'RR. Similarly, Blimp1 indirectly controls the chromatin accessibility of all 3' enhancer in the *Igk* locus.

The transcription factor XBP1 is essential for efficient antibody secretion of plasma cells5. As shown here, *Xbp1* transcription is strongly activated in a Blimp1-dependent manner in plasmablasts, although we could not detect Blimp1-binding sites in the vicinity of the *Xbp1* gene. It is therefore conceivable that *Xbp1* is indirectly activated by the UPR3, which is induced by the increased synthesis of secreted immunoglobulins in plasmablasts.

IRF4 is another essential regulator of plasma cell development7, which is known to bind to and activate the *Prdm1* (Blimp1) gene at the onset of plasmablast differentiation9,10. Here we have identified *Irf4* as one of 7 Blimp1-activated transcription factor genes that was directly activated by Blimp1 even in the absence of protein synthesis in OHT-treated WEHI-Blimp1-ER^{T2} B-cells. Hence, Blimp1 and IRF4 cross-regulate each other's expression in antibody-secreting cells. IRF4 recognizes its motif (5'-GAAA-3') with high affinity only upon cooperative binding with the Ets protein PU.1 to the Ets-IRF composite element EICE31 or with the BATF-Jun complex to the AP1-IRF composite element AICE51. Interestingly, the IRF4 recognition sequence is also present in the Blimp1-binding motif. Moreover, half of all Blimp1 peaks overlap with IRF4 and PU.1 peaks in plasmablasts, while a subset of these peaks contains a common binding site for Blimp1 and the PU.1/IRF4 complex. However, this common binding site is bound by Blimp1 and the PU.1/IRF4 complex in a mutually exclusive manner, thus excluding the possibility that Blimp1 and IRF4 cooperatively bind to DNA.

Blimp1 is known to function as a transcriptional repressor11. Here, we have identified the full spectrum of repressed Blimp1 target genes, which confirmed and extended previous data by demonstrating that the four transcription factor genes *Pax5* (ref. 21), *Ciita*15,22, *Spib*15 and *Id3* (ref. 15) are directly repressed by Blimp1 in plasmablasts. The mutual antagonism of Pax5 and Blimp1 in late B-cell development is of particular interest, as Pax5 maintains the identity of mature B-cells52, whereas Blimp1 enforces the plasma cell fate8,14. Consequently, the Blimp1-dependent repression of *Pax5* in plasma cells interferes with the B-cell fate through indirect loss of the expression of Pax5 target genes, many of which code

for B-cell-specific cell surface receptors, signal transducer and transcriptional regulators in mature B-cells26.

The identification of several regulated Blimp1 target genes with functions in cell adhesion and migration has defined a novel Blimp1-regulated pathway. Blimp1 represses 23 genes coding for chemokine receptors (Ackr2, Ccr7), cell adhesion proteins (Cd37, Chd17, Itgam, Sell [CD62L]), intracellular adaptors (Ahnak, Nckipsd, Pstpip1), GTPase-activating proteins (Arhgap17, Arhgap24, Asap1), GTPases (Gbp1, Gbp2), a guanine nucleotide-exchange factor (Fdg2), a kinase (Hck), a metabolic enzyme (St3gal6), an E3 ligase subunit (Asb2) and cytoskeleton-associated proteins (Evl, Gsn, Myo1e, Rcsd1, Tmsb4x). Blimp1 also activated 9 genes coding for cell surface proteins (Alcam, Ccrl2), intracellular adaptors (Nck2, Rasip1, Tns3), GTPase-activating proteins (Dab2ip, Evi5), a guanine nucleotide-binding protein (Gnaz) and an actin-bundling molecule (Pls1), further demonstrating that genes involved in cell adhesion and migration undergo a radical change in expression during the B-cell-to-plasmablast transition. Consistent with these expression changes, Blimp1 controls the increased migration and adhesion of plasmablasts, which explains the previously described migratory and sessile behavior of plasmablasts and plasma cells in the spleen30, lymph node29,30 and bone marrow29,30

At the chromatin level, Blimp1 induces the rapid loss of active histone modifications and a delayed gain of the repressive H3K27me3 mark at binding sites of repressed target genes. The spreading of H3K27me3 from these Blimp1-binding sites strictly depends on Blimp1, but does not require the presence of a CpG island. This finding is incompatible with the prevailing model that the H3K27-methylating PRC2 complex is recruited by default to CpG islands (CGI) lacking active chromatin43. Instead, we demonstrate that Blimp1 binds to and recruits the PRC2 complex in an instructive manner to Blimp1-binding sites at repressed target genes. In addition to PRC2, Blimp1 was shown, mainly in non-B-lymphoid cell types, to interact with Groucho proteins18, histone deacetylases19, the H3K9 methyltransferase G9a17 and the H3K4 demethylase LSD1 (ref. 16), which could act as co-repressors to mediate Blimp1-dependent gene silencing. Here we discovered a different set of Blimp1-interacting complexes in plasmablasts by Blimp1-Bio pulldown experiments and mass-spectrometric identification of subunits of the chromatin-remodeling BAF45 and NuRD45 complexes as well as of the histone-deacetylating NCoR46 and SIN346 co-repressor complexes. Importantly, Blimp1 rapidly recruited these complexes to its binding sites at repressed target genes in WEHI-Blimp1-ER^{T2} B-cells. Hence, Blimp1 represses its target genes in plasmablasts and plasma cells by recruiting chromatin-remodeling and histone-modifying complexes to its binding sites.

Online Methods

Mice

The *Prdm1*$^{fl/fl}$ mice1, *Prdm1*$^{Gfp/+}$ mice2, *Meox2*$^{Cre/+}$ mice3, transgenic FLPe mice4 and transgenic *Cd23*-Cre mice5 were maintained on the C57BL/6 genetic background. All animal experiments were carried out according to valid project licenses, which were approved and regularly controlled by the Austrian Veterinary Authorities.

Generation of the *Prdm1*^{Bio} allele

The targeting vector for generating the *Prdm1*^{ihCd2} allele was obtained by insertion of the following sequences in the 5' to 3' direction (Supplementary Fig. 2a) into the *Prdm1* bacterial artificial chromosome (BAC) bMQ-126012 by recombination-mediated genetic engineering in *E. coli*; a 217-bp MfeI-AscI fragment containing C-terminal tag sequences (fused in frame to the last *Prdm1* codon), a 1.8-kb AscI-SalI fragment containing the IRES-hCd2 (ihCd2) reporter gene (flanked by *frt* sites) and a 1.9-kb SalI-BamHI fragment containing the promoter of the mouse phosphoglycerate kinase (*Pgk1*) promoter linked to the neomycin (Neo) resistance gene (flanked by *loxP* sites). The tag sequences contained epitopes for Flag and V5 antibodies, two cleavage sites for the TEV protease and a biotin acceptor sequence (Biotin) for biotinylation by the *Escherichia coli* biotin ligase BirA6. In a second step, the *Prdm1*^{ihCd2} targeting vector was generated by excision and insertion of the integrated sequences together with the flanking 5' (5.0 kb) and 3' (1.8 kb) homology regions by recombination-mediated genetic engineering from the modified BAC into the pBV-DTA-pA plasmid containing a gene encoding the herpes simplex virus thymidine kinase (for negative selection). DNA (15 μg) linearized with SgrA1 was transfected by electroporation into cells ($1x10^7$) of the hybrid C57BL/6 x 129Sv ES cell line A9, followed by selection with 250 μg/ml G418. PCR-positive clones were verified by Southern blot analysis (Supplementary Fig. 2b) before injection into C57BL/6 blastocysts and the generation of *Prdm1*$^{ihCd2\text{-}Neo/+}$ mice. The *Prdm1*^{ihCd2} allele was obtained by crossing *Prdm1*$^{ihCd2\text{-}Neo/+}$ mice with *Meox2*$^{Cre/+}$ mice3 and the *Prdm1*^{Bio} allele by subsequent crossing with transgenic FLPe mice4 mice. The following primers were used for PCR genotyping of *Prdm1*$^{Bio/+}$ mice: 5'-GCTGCCTTTGGAGGATCTGA-3' (a), 5'- AGGAAGGCGCTATGCAAACA-3' (b). The *Prdm1*^{Bio} allele was identified as a 1049-bp PCR fragment and the wild-type *Prdm1* allele as 648-bp PCR fragment by using the primer pair a/b.

Generation of the *Spi1*^{Bio} allele

The same strategy described above was also employed for the generation of the *Spi1*^{Bio}allele, containing the same C-terminal tag sequences with the additional insertion of a PreScission (PreSc) cleavage site (Supplementary Fig. 4d), by using the *Spi1* (PU.1) BAC bMQ-47L24 for recombination-mediated genetic engineering in *E. coli*. The following primers were used for PCR genotyping of *Spi1*$^{Bio/+}$ mice: 5'-CTTCCAGTTCTCGTCCAAGC-3' (a), 5'-GGCGACGGGTTAATGCTAT-3' (b). The *Spi1*^{Bio} allele was identified as a 694-bp PCR fragment and the wild-type *Spi1* allele as a 279-bp PCR fragment by using the primer pair a/b.

Antibodies

The following monoclonal antibodies were used for flow cytometric analysis of the mouse spleen, lymph node and bone marrow: B220/CD45R (RA3-6B2), CD1d (1B1), CD2 (RM2-5), CD3ε (145-2C11), CD4 (GK1.5), CD8a (53-6.7), CD11b/Mac1 (M1/70), CD16/32 (2.4G2), CD19 (1D3), CD21/CD35 (7G6), CD22 (Cy34.1), CD23 (B3B4), CD25/IL-2Rα (PC61), CD28 (37.51), CD38 (90), CD44 (IM781), CD49b (DX5), CD93/AA4.1 (PB493), CD95 (FAS), CD115/MCSF-R (AFS98), CD117/c-Kit (2B8), CD127/IL-7Rα (A7R34), CD135/Flt3 (A2F10.1), CD138 (281-2), CXCR4 (2B11), F4/80 (CI:A3-1), Gr1

(RB6-8C5), IgD (11.26c), IgG1 (A85-1), IgM (II/41), IgM^b (AF6-78), NK1.1 (PK136), Ly6C (6C3), Sca1/Ly6A (D7), TCRβ (H57-597), Ter119 (TER119) and human CD2 (RPA-2.10) antibodies.

The following antibodies were used for immunoblot or immunoprecipitation analyses: anti-Blimp1 (rat mAb clone 7E5; from Stephen Nutt, WEHI Melbourne), anti-Brg1 (mouse mAb clone G-7; Santa Cruz), anti-Brg1 (rabbit polyclonal Ab; from Robert Kingston, Massachusetts General Hospital, Boston), anti-CHD4 (mouse mAb clone 3F2/4; Abcam), anti-CHD4 (rabbit polyclonal Ab A301-081; Bethyl laboratories), anti-ER (rabbit polyclonal Ab HC-20; Santa Cruz), anti-Ezh2 (rabbit mAb clone D2C9; Cell Signaling), anti-HDAC1 (mouse mAb clone 10E2; Abcam), anti-HDAC1 (rabbit polyclonal Ab H-51; Santa Cruz), anti-IRF4 (goat polyclonal Ab M-17; Santa Cruz), anti-MBD3 (rabbit polyclonal Ab A302-528; Bethyl laboratories), anti-Myc (mouse mAb clone 9E10; produced in-house), anti-NCOR1 (rabbit polyclonal Ab ab24552; Abcam), anti-PU.1 (rabbit polyclonal Ab T-21; Santa Cruz), anti-SIN3A (rabbit polyclonal Ab AK-11; Santa Cruz) and anti-V5 (mouse mAb clone 5C5; produced in-house).

Antibodies recognizing the following histone tail modifications were used for ChIP analysis: anti-H3K4me2 (rabbit polyclonal Ab 07-030; Merck Millipore), anti-H3K4me3 (rabbit polyclonal Ab pAb-003-050; Diagenode), anti-H3K9ac (rabbit polyclonal Ab 07-352; Merck Millipore), anti-H3K27ac (rabbit polyconal Ab ab4729; Abcam), H3K27me3 (rabbit polyclonal Ab; from T. Jenuwein, MPI Freiburg), H3K27me3 (rabbit mAb 9733; Cell Signaling).

Flow cytometric sorting of B cells, plasmablasts and plasma cells

Mature B cells from lymph nodes, long-lived plasma cell from the bone marrow and in vitro differentiated activated B cells and plasmablasts were sorted with a FACS Aria machine (Becton Dickinson) as follows: mature B cells ($B220^+CD19^+IgM^{lo}IgD^{hi}$), *Prdm1*$^{Gfp/+}$ plasma cells ($Lin^-GFP^{hi}B220^{lo}CD138^{hi}CD28^+$), activated *Prdm1*$^{Gfp/+}$ B cells ($GFP^-B220^+CD138^-$), *Prdm1*$^{Gfp/+}$ pre-plasmablasts (GFP^+CD138^-), *Cd23*-Cre *Prdm1*$^{Gfp/fl}$ pre-plasmablasts ($GFP^+CD138^-CD22^+$) and *Prdm1*$^{Gfp/+}$ plasmablasts (GFP^+CD138^+). The lineage (Lin) marker antibodies contained anti-CD4, anti-CD8a, anti-CD21 and anti-F4/80 antibodies for sorting of plasma cells.

In vitro differentiation of plasmablasts

Our standard LPS stimulation procedure resulted in 40% pre-plasmablasts/plasmablasts and 60% activated B cells at day 4 of LPS treatment. For this, B cells from the spleen and lymph nodes were isolated as $B220^+$ cells by immunomagnetic sorting and seeded at a density of 1 x 10^6 cells/ml in DMEM medium containing 10% fetal calf serum (Sigma 080M3395) and 25 μg/ml LPS (L4130 Sigma-Aldrich). Our improved LPS stimulation condition led to 80% pre-plasmablasts/plasmablasts and 20% activated B cells at day 4 of LPS treatment. For this, the sorted $B220^+$ B cells were seeded at a lower cell density of 5 x 10^4 cells/ml in DMEM medium containing 10% fetal calf serum (GE Healthcare A15-101) and 25 μg/ml LPS (L4130 Sigma-Aldrich).

Immunization and ELISPOT assay

The immune response to a specific antigen was studied by intraperitoneal injection of 100 μg of 4-hydroxy-3-nitrophenylacetyl-conjugated keyhole limpet hemocyanin (in alum). The frequencies of anti-NP-IgG1 antibody-secreting cells (ASCs) were determined in the spleen and bone marrow by enzyme-linked immunospot (ELISPOT) assay as described7. NP_4-BSA- and NP_{23}-BSA-coated plates were used for capturing high-affinity or total anti-NP-IgG1 antibodies secreted by individual cells, respectively. Spots were visualized with goat anti-mouse IgG1 antibodies conjugated to alkaline phosphatase (Southern Biotechnology Associates), and color was developed by the addition of BCIP/NBT Plus solution (Southern Biotechnology Associates). After extensive washing, the spots were counted with an AID ELIspot reader system (Autoimmun Diagnostika).

Transwell migration assay

Activated B cells and pre-plasmablasts were isolated by flow cytometric sorting (as described above) at day 4 of LPS stimulation and resuspended at $4x10^6$ cells/ml in IMDM medium supplemented with 10% heat-inactivated fetal calf serum, 1 mM glutamine and 50 μM β-mercaptoethanol. The suspension of $0.4x10^6$ cells (100 μl) was placed in the upper compartment and DMEM medium (600 μl) containing 400 ng/ml recombinant CXCL12 (SDF-1α; R&D Systems) in the lower compartment of a transwell chamber (5 μm pore size; Corning Inc.). After incubation at 37°C for 2 h, the cells migrating into the lower chamber were counted using a Casy cell counter, and their percentage relative to the total cells was calculated.

Adhesion assay

The adhesion of sorted activated B cells and pre-plasmablasts to ICAM1- or VCAM1-coated slide was analyzed as follows. Eight-well chamber slides (Thermo Scientific) were coated with recombinant mouse VCAM1-Fc protein or ICAM1-Fc protein (25 μg/ml; R&D Systems) for 1.5 h at room temperature and washed 3 times with PBS. The sorted cells were washed and resuspended in IMDM medium supplemented with 10% heat-inactivated fetal calf serum, 1mM glutamine, 50 μM β-mercaptoethanol and 100 ng/ml CXCL12 (SDF-1α; R&D Systems), and subsequently $1x10^5$ cells in 200 μl were seeded into each well. Following incubation for 6 h at 37°C, the chambers were removed and slides were washed with pre-warmed medium and then with PBS. Fixation of the cells was performed with 4% paraformaldehyde for 15 min at room temperature. The slides were washed 3 times with PBS, stained with 0.1% Crystal Violet for 30 min prior to washing with distilled water and drying. Following dehydration and embedding of the samples, images of each well were acquired. The number of cells that were attached to the glass slides was automatically counted to determine the cell number per cm^2.

Cloning of expression constructs

For transient transfection experiments, we cloned full-length cDNA coding for different transcription factors into one of the two expression vectors pRK7 and pKW2T containing a CMV enhancer/promoter region, a polylinker, an SV40 polyadenylation sequence and an SV40 (pRK7) or Polyomavirus (pKW2T) replication origin8. The following expression

vectors were cloned: pCMV-mBlimp1-Bio-IRES-BirA (*Blimp1* cDNA with C-terminal biotin acceptor sequence linked to an IRES-BirA expression cassette in pRK7); pCMV-mBlimp1 (mouse *Blimp1* cDNA in pRK7); pCMV-myc-hEzh2 (N-terminal Myc tag linked to human *EZH2* cDNA in pRK7); pCMV-mEed (mouse *Eed* cDNA in pRK7); pCMV-hSuz12 (human *SUZ12* cDNA in pRK7); pCMV-myc-mIrf4 (N-terminal Myc tag linked to mouse *Irf4* cDNA in pRK7); pCMV-flag-mPU.1 (N-terminal Flag tag linked to mouse *Sfi1* [PU.1] cDNA in pKW2T). The retroviral MiCD2-Blimp1-ER^{T2} vector was generated by coupling full-length mouse *Blimp1* cDNA with the mutant ligand-binding domain of the human estrogen receptor (ER^{T2})9 via a double-stranded oligonucleotide coding for the amino acid linker indicated in bold: Blimp1-PMDP-**QLAAAAAAADP**-SAGD-ER. The Blimp1-ER^{T2} cDNA was inserted into the retroviral vector MiCD210 upstream of the IRES-hCD2 indicator gene.

Generation and stimulation of WEHI-Blimp1-ER^{T2} cells

Murine WEHI-231 B cells were infected with the MiCD2-Blimp1-ER^{T2} retrovirus and selected for high expression of human CD2, followed by single-cell cloning. Clones, which showed the highest degree of activation and repression of selected Blimp1 target genes after 16 h of stimulation with 4-hydroxytamoxifen (OHT, 1 μM), were selected and used for further analysis.

For OHT induction experiments (Fig. 2f-h, Fig. 4e and Fig. 8e,f), cell of the WEHI-Blimp1-ER^{T2} cell clone 194 were plated at a concentration of 1-2x10^{6} cells/ml and were then treated with OHT (1 μM) for the indicated time. For gene expression analysis (Fig. 2f), cells were preincubated with cycloheximide (CHX; 25 mg/ml) for 30 min prior to the addition of OHT for 6h, where indicated.

RT-qPCR analysis of mRNA and primary transcripts

Total RNA was prepared from OHT-treated WEHI-Blimp1-ER^{T2} cells or LPS-stimulated activated B cells and plasmablasts by using the RNeasy Mini Kit (Qiagen) with an additional DNase I treatment. The cDNA was synthesised using the Random Primer Mix (New England Biolabs) and SuperScript® III Reverse Transcriptase (Life Technologies). Nascent transcripts of selected genes were measured by qPCR using primers, that are located in intronic gene regions (Supplementary Table 5), and were normalised against nascent *Tbp* transcripts (first intron).

Identification of Blimp1-interacting proteins by mass spectrometry

LPS-stimulated *Blimp1*$^{Bio/Bio}$ *Rosa26*$^{BirA/BirA}$ or control *Rosa26*$^{BirA/BirA}$ plasmablasts were used to prepare nuclear extracts followed by protein precipitation with streptavidin Dynal beads (M280; Invitrogen). On-bead digest of the isolated proteins was performed with trypsin. The nano-HPLC (high-performance liquid chromatography) system used for the separation and analysis of the tryptic peptides was an UltiMate 3000 RSLC nano system (Thermo Fisher Scientific) coupled to a Q Exactive mass spectrometer (Thermo Fisher Scientific), equipped with a Proxeon nanospray source (Thermo Fisher Scientific). The Q Exactive mass spectrometer was operated in data-dependent mode, using a full scan (m/z range 380-1650, nominal resolution of 70 000, target value 3E6) followed by MS/MS scans

of the 12 most abundant ions. For peptide identification, the RAW-files were loaded into Proteome Discoverer (version 1.4.0.288, Thermo Scientific). All hereby created MS/MS spectra were searched using Mascot 2.2.07 (Matrix Science, London, UK) against the Swissprot protein sequence database, using the taxonomy mouse (July 2014, 16678 sequences). The peptide mass tolerance was set to ± 5 ppm and the fragment mass tolerance to ± 0.03 Da. The maximal number of missed cleavages was set to 2. The result was filtered to 1% FDR using Percolator algorithm integrated in Proteome Discoverer.

Nuclear extract preparation and co-precipitation analysis

Nuclear extracts were prepared as described previously11 with minor modifications. Briefly, 5-6x10^8 in vitro LPS-differentiated plasmablasts or transfected HEK-293T cells were lysed in a buffer consisting of 10 mM Tris pH 8.0, 0.32 M sucrose, 50 mM KCl, 20 mM NaCl, 3 mM $CaCl_2$, 2 mM magnesium acetate (MgAc), 0.1% NP-40, 2 mM 6-aminocaproic acid (6AA), 0.15 mM spermine, 0.5 mM spermidine, 0.5 mM PMSF and 0.1% protease inhibitor cocktail, and the nuclei were collected by centrifugation for 5 min at 500 xg. Pelleted nuclei were then resuspended in low salt buffer consisting of 10 mM HEPES pH 7.9, 20% glycerol, 2 mM MgAc, 20 mM KCl, 1%NP-40, 10 mM NaF, 2 mM 6AA, 0.5 mM PMSF and 0.1% protease inhibitor cocktail. Slowly the same amount of high salt buffer (0.70 M KCl) was added to lyse the nuclei. The Benzonase^R endonuclease (1.8 µl with 250 units/µl; Merck) was immediately added to 800 µl of the nuclei suspension corresponding to 1x10^8 cells followed by incubation at 4°C for 45 min and centrifugation at 16,000 xg for 10 min. The protein content of the nuclear extract was measured by Bradford assay (BioRad) using BSA as a standard. The extract was diluted with 1 volume of low salt buffer (see above) prior to streptavidin pulldown or immunoprecipitation.

Dynabeads were blocked with 1 mg/ml BSA in PBS overnight at 4°C. Nuclear extracts were precleared with protein G Dynabeads for 1h at 4°C and subsequently incubated with streptavidin Dynabeads (M280; Invitrogen) or with purified antibodies at 4°C overnight. In the latter case, protein A Dynabeads (Invitrogen) were subsequently added for another 3 h. The beads were washed 5 times in 20 mM Tris pH 8, 250 mM KCl, 1.5 mM MgCl2, 10% glycerol, 2 mM 6AA, 10 mM NaF, 1 mM β-glycerophosphate, 1 mM sodium pyrophosphate and 0.1% protease inhibitor cocktail by removing the supernatant by magnetic sorting. The precipitated proteins were resuspended in 2x SDS sample buffer, eluted from the beads by boiling and separated by SDS-PAGE followed by Western blotting.

For co-precipitation of PRC2 with Blimp1-Bio (Fig. 8b,c), 1.5x10^7 HEK-293T cells were transiently transfected by Lipofectamine (Invitrogen) with the expression plasmids pCMV-mBlimp1-Bio-IRES-BirA (1 µg), pCMV-myc-hEzh2 (1µg), pCMV-hSuz12 (1 µg) and pCMV-mEed (1µg) prior to nuclear extract preparation.

Electrophoretic mobility shift assays

Nuclear extracts were prepared from HEK-293T cells that were transiently transfected with an expression vector for Blimp1 (pCMV-mBlimp1-Bio-IRES-BirA), PU.1 (pCMV-flag-mPU.1) or IRF4 (pRK7-myc-mIrf4). Double-stranded oligonucleotides corresponding to the common binding motif of the *Vkr2* and *Tlr9* genes were end-labeled by T4 polynucleotide

kinase. For analysis of protein binding, the labeled probe (20 fmoles) was incubated with 8 μg of nuclear extract in 20 μl of binding buffer (20 mM HEPES pH 7.9, 50 mM KCl, 1 mM DTT, 1.5 mM MgAc, 2 mM 6AA, 1x cOmplete Protease Inhibitor Cocktail (Roche), 5% glycerol, 4% Ficoll, 0.15 μg/μl poly[d(I-C)]) for 30 min at room temperature. For super-shift analysis, 1-2 μg of anti- IRF4, anti-PU.1 or anti-V5 antibody were added to the binding reaction. Protein-DNA complexes were separated on a 4% polyacrylamide gel in 0.25x TBA buffer (22 mM Tris-borate pH 8.3, 2 mM 6AA) at 150 V for 3 h at 25°C. Gels were fixed, dried and subjected to autoradiography. The following binding sites were used for EMSA: *Vkr2* intron 1 oligonucleotides:

5'-CAATACTTTCTCTTCCCCACATGAAC-3' and 5'-GTTCATGTGGGGAAGAGAAAGTATTG-3'; *Tlr9* intron 1 oligonucleotides: 5'-AGAGGAGAGGAAGAGAAAGTGGGAGA-3' and 5'-TCTCCCACTTTCTCTTCCTCTCCTCT-3'.

Mapping of open chromatin regions by ATAC-seq

Open chromatin regions (referred to as DHS sites) were mapped in activated B cells and plasmablasts by the ATAC-seq method as described12 with the following modification. The nuclei were prepared by incubating cells with nuclear preparation buffer (0.30 M sucrose, 10 mM Tris pH 7.5, 60 mM KCl, 15 mM NaCl, 5 mM $MgCl_2$, 0.1 mM EGTA, 0.1% NP40, 0.15 mM spermine, 0.5 mM spermidine, 2 mM 6AA) prior to the Tn5 treatment (20,000 cells with 4 μl of the Nextera Tn5 transposase).

ChIP-seq and ChIP-qPCR analysis of histone modifications

For ChIP-seq analysis, sorted activated B cells and plasmablasts after 4 days of LPS stimulation were used for chromatin immunoprecipitation (ChIP) with histone modification-specific antibodies (see antibody section above), as described in detail13. The ChIP efficiency was quantified by real-time PCR analysis and about 1-5 ng of ChIP-precipitated DNA was used for library preparation. The ChIP-qPCR analysis of histone modifications (Fig. 2g,h) was performed using OHT-treated WEHI-Blimp1-ER^{T2} cells, and the precipitated DNA was subjected to the qPCR quantification, using region-specific primers listed in Supplementary Table 6. The specific enrichment was calculated as the DNA amount relative to the input followed by normalization against the *Tbp* promoter.

ChIP-qPCR analysis of histone-modifying and chromatin-remodeling factors

WEHI-Blimp-ER^{T2} cells were treated with OHT (1 μM) for a short period of time (0.5-2 h) in a 50 ml conical tube and were then subjected to crosslinking first with 1% formaldehyde (Sigma) for 10 min followed by 2 mM disuccinimidyl glutarate (DSG; Pierce) for 45 min. The nuclei were prepared and lysed in the presence of 0.1% SDS. The chromatin was sheared by sonication with the Bioruptor® Standard (Diagenode), followed by immunoprecipitation with specific antibodies. The precipitated DNA was subjected to the qPCR quantification, using primers listed in Supplementary Table 6. The specific enrichment was measured and caliculated as the DNA amount relative to the input followed by normalization against the *Tbp* promoter.

Bio-ChIP-seq analysis of Blimp1 binding

CD138^{+} plasmablasts were generated by LPS-induced differentiation of mature B cells from *Prdm1*$^{Bio/Bio}$ *Rosa26*$^{BirA/BirA}$ or *Spi1*$^{Bio/Bio}$ *Rosa26*$^{BirA/BirA}$ mice. Chromatin from ~1x10^{8} plasmablasts was prepared using a lysis buffer containing 0.25% SDS prior to chromatin precipitation by streptavidin pulldown (Bio-ChIP), as described14. The precipitated genomic DNA was quantified by real-time PCR, and about 1-5 ng of ChIP-precipitated DNA was used for library preparation.

cDNA preparation for RNA-sequencing

RNA from LPS-differentiated activated B cells, pre-plasmablasts and plasmablasts as well as ex vivo sorted lymph node B cells and bone marrow plasma cells was isolated with the RNeasy Plus Mini Kit (Qiagen), and mRNA was obtained by two rounds of poly(A) selection using the Dynabeads mRNA purification kit (Invitrogen) followed by fragmentation by heating at 94°C for 3 min (in fragmentation buffer). The fragmented mRNA was used as template for first-strand cDNA synthesis with random hexamers using the Superscript Vilo First-Strand Synthesis System (Invitrogen). The second-strand cDNA was synthesized with 100 mM dATP, dCTP, dGTP and dUTP in the presence of RNase H, *E. coli* DNA polymerase I and DNA ligase (Invitrogen). The incorporation of dUTP allowed elimination of the second strand during library preparation (see below), thereby preserving strand specificity15.

Library preparation and Illumina deep sequencing

About 1-5 ng of cDNA or ChIP-precipitated DNA were used as starting material for the generation of sequencing libraries with the NEBNext Quick Ligation Module, NEBNext Endrepair Module and NEBNext dA-Tailing module or NEBNext Ultra Ligation Module and NEBNext End Repair/dA-Tailing module. DNA fragments of the following sizes were selected for the different experiments: 200–500 bp for ChIP-seq and 150–700 bp for RNA-seq with AMPure XP beads (Beckman Coulter). For strand-specific RNA-sequencing, the uridines present in one cDNA strand were digested with uracil-N-glycosylase (New England Biolabs) as described15 followed by PCR amplification with the KAPA Real Time Amplification kit (KAPA Biosystems). Completed libraries were quantified with the Agilent Bioanalyzer dsDNA 1000 assay kit and Agilent QPCR NGS Library Quantification kit. Cluster generation and sequencing was carried out by using the Illumina HiSeq 2000 system with a read length of 50 nucleotides according to the manufacturer's guidelines. Supplementary Table 7 provides further information about all sequencing experiments of this study.

Sequence alignment

Sequence reads that passed the Illumina quality filtering were considered for alignment. For ChIP-seq, the remaining reads were aligned to the mouse genome assembly version of July 2007 (NCBI37/mm9), using the Bowtie program version 12.5. For ATAC-Seq, the Bowtie program version 2.1.0 was used with additional parameters -sensitive -X 5000.

Peak calling of ChIP-seq data and target gene assignment

We used three different peak finder tools, depending on the specific need of the subsequent analysis. (1) For determining the regulatoy landscape and overall number of peaks, we used the MACS program version 1.3.6.1 (ref. 16) with default parameters, a genome size of 2,654,911,517 bp (mm9) and a mixture of pro-B and mature B cell input control sample. Peaks were filtered for *P* values of < 10^{-10}. This stringent cutoff efficiently removed false positive (unique) peaks of technical replicas. Blimp1 peaks were assigned to target genes as described17. (2) For H3K27me3 ChIP-seq samples, we used the SICER program18, as it performs best for broad peaks. (3) For de novo motif prediction analysis, we used the SISSRS program19, which reports the transition point (peak center), which we extended by 150 bp on both sides to obtain 300 bp peaks. Both the peaks and peak centers overlapped well with peaks and summits reported by MACS (data not shown).

Read density heat maps

Read densities were calculated using the JNOMICS program[I. Tamir, unpublished]. Associated heat map visualizations were implemented using R (http://www.R-project.org) and were wrapped with customized bash scripts for command line usage.

Motif discovery

For motif discovery, we used the MEME-ChIP suite (version 4.9.1)20 to discover the most significant motif in the top 300 SISSRS peaks of each track or track overlap subset. The individual overlap subsets of SISSRS peaks were then scanned with these predicted motifs using FIMO (also MEME-ChIP suite) with a *P* value < 0.00005. Regions with overlapping motif matches were extracted and aligned using MAFFT (version 6.910)21 to determine the common binding motif for Blimp1 and the PU.1-IRF4 complex (Fig. 4d and Supplementary Fig. 4a). The resulting multiple sequence alignments were visualized using WebLogo (version 3.3)22. For the analysis of all Blimp1 peaks, the FIMO *P* value threshold was set such that no more than 20% of randomly selected DHS sites (excluding overlapping Blimp1 peaks) had a motif match (Fig. 2c).

Peak overlap analysis

All peak overlap analyses were performed with the Multovl program23 by using a minimal overlap length of one and allowing for all possible overlaps. Results were parsed and converted to tables with custom-made bash, perl and R scripts and analyzed using the TIPCO Spotfire program (version 5.0.1). Venn diagrams were produced with eulerAPE (version 3.0.0)24.

CpG island analysis

To display the CpG read densities and profiles shown in Fig. 7b-d, all reads of the mouse CAP-seq sample GSM535958 (m_BloodLowNaCl_CXXC_M)25 of the NCBI GEO series GSE21442 were aligned as described above. This resulted in 13.9 million of aligned reads, which were then used as input for the plotting procedures. The CpG island overlap analysis shown in Supplementary Fig. 7e was based on a union of the mouse Bio-CAP peaks26

deposited in the NCBI GEO series GSE43512 (sample GSM1064678 [testis], GSM1064679 [liver] and GSM1064680 [embryonic stem cell V6.5]).

ATAC-seq data processing

Insert sizes were extracted from the aligned BAM files with samtools (version 0.1.18) and analyzed with R (version 3.1.1) to determine the fragment sizes associated with nucleosome-free positions. After removing fragments above 1 kb, a random subsample of 50,000 values was drawn from each alignment. The h.crit function from the silvermantest package (version 1.0) was used to determine the bandwidth for k=6 modes in the density function of the fragment size distribution. These modes were used as means for fitting k=6 normal distributions to the observed fragment sizes, using the normalmixEM function from the mixtools package version 1.0.2. With these parameters, the fragment size boundaries were fixed so that no more than 80% of each partition overlapped with its neighbors, analogous to the analysis performed by Buenrostro et al. (ref. 12). Only the first reads of read pairs with an estimated fragment size below 150 nucleotides have been used for calling peaks using MACS as described above.

Analysis of RNA-seq data

For analysis of differential gene expression, the RNA-seq samples were cut down to a read length of 44 bp and aligned to the mouse transcriptome using the TopHat version 1.4.1 (ref. 27). Details about the transcriptome analysis were previously described17. The number of reads per gene was counted using the HTseq version 0.5.3 (ref. 28) with the overlap resolution mode option set to ‘union’. Initial quality assessment showed strong batch effects between the two sets of in vitro RNA-seq samples performed on different days. By normalizing for the GC content bias across those eight samples, this between-batch variation was drastically reduced. The normalization was done using the R package EDAseq 1.0.0 (ref. 29). Genes with less than 10 counts per sample on average were excluded. For the remaining genes, all RefSeq transcripts assigned to the same gene were investigated, and cases, where the GC content differed by 10% or more between transcripts assigned to the same gene, were removed. If the difference was smaller than 10%, the average GC content across the transcripts were used as GC content input to EDASeq. EDASeq was run with default parameters. The GC-normalized EDAseq output was rounded, and the results were used as input for the downstream count-based analysis. The ex vivo samples showed no batch effect, and no GC normalization was performed. The ex vivo and in vitro data were analyzed separately using the R package DESeq version 1.8.3 (ref. 30). To this end, the samples were normalized, and the dispersions were estimated using the default DESeq settings. DESeq was then used to identify differentially expressed genes for each pairwise comparison of interest. Genes with an adjusted P value of < 0.1 were called as differentially expressed. Due to the strong batch effects in the in vitro data set, RPM and RPKM were not calculated. Instead, the GC-normalized rounded counts (EDAseq output) were used to calculate the GC-normalized RPM and GC-normalized RPKM. The calculations were done as for RPM and RPKM with the only difference that the GC-normalized data was used instead of the raw counts (for further information see Supplementary Table 7).

For the detailed expression analysis of the *Igh* and *Igk* loci (Fig. 6 and Supplementary Fig. 6), the transcriptome annotation was updated to include the immunoglobulin genes. V, D, J and C segments were incorporated from Ensembl release 67 (ref. 31). IghM, IghD, IghG, IghE and IghA were manually curated to provide detailed exon annotations and were split into constant, membrane, secreted, hinge and I exon regions. The number of reads per gene (or per gene region in the case of the *Igh* locus) was used to calculate the GC-normalized RPM and RPKM for the in vitro data as described above. Ratios between secreted and membrane *Igh* transcripts were subsequently estimated by using the GC-normalized RPKM ratios of the secreted and membrane regions.

Supplementary information

Refer to Web version on PubMed Central for supplementary material.

Acknowledgments

We thank Daniela Kostanova Poliakova for technical assistance, K. Aumayr and her team for flow cytometric sorting, K. Mechtler and his team for mass spectrometry analysis as well as A. Sommer and his team at the Campus Science Support Facilities for Illumina sequencing. This research was supported by Boehringer Ingelheim and an ERC Advanced Grant (291740-LymphoControl) from the European Community's Seventh Framework Program. Research of the Tarakhovsky laboratory was supported by the Emerald Foundation, and research of the Nutt laboratory by fellowships from the National Health and Medical Research Council of Australia, IRIISS grant #361646, Program Grant #1054925 and a Multiple Myeloma Research Foundation Senior Award.

References

1. Nutt SL, Hodgkin PD, Tarlinton DM, Corcoran LM. The generation of antibody-secreting plasma cells. Nat Rev Immunol. 2015; 15:160–171. [PubMed: 25698678]
2. Shi W, et al. Transcriptional profiling of mouse B cell terminal differentiation defines a signature for antibody-secreting plasma cells. Nat Immunol. 2015; 16:663–673. [PubMed: 25894659]
3. Yoshida H, Matsui T, Yamamoto A, Okada T, Mori K. XBP1 mRNA is induced by ATF6 and spliced by IRE1 in reponse to ER stress to produce a highly active transcription factor. Cell. 2001; 107:881–891. [PubMed: 11779464]
4. Shaffer AL, et al. XBP1, downstream of Blimp-1, expands the secretory apparatus and other organelles, and increases protein synthesis in plasma cell differentiation. Immunity. 2004; 21:81–93. [PubMed: 15345222]
5. Reimold AM, et al. Plasma cell differentiation requires the transcription factor XBP-1. Nature. 2001; 412:300–307. [PubMed: 11460154]
6. Taubenheim N, et al. High rate of antibody secretion is not integral to plasma cell differentiation as revealed by XBP-1 deficiency. J Immunol. 2012; 189:3328–3338. [PubMed: 22925926]
7. Mittrücker H-W, et al. Requirement for the transcription factor LSIRF/IRF4 for mature B and T lymphocyte function. Science. 1997; 275:540–543. [PubMed: 8999800]
8. Shapiro-Shelef M, et al. Blimp-1 is required for the formation of immunoglobulin secreting plasma cells and pre-plasma memory B cells. Immunity. 2003; 19:607–620. [PubMed: 14563324]
9. Sciammas R, et al. Graded expression of interferon regulatory factor-4 coordinates isotype switching with plasma cell differentiation. Immunity. 2006; 25:225–236. [PubMed: 16919487]
10. Kwon H, et al. Analysis of interleukin-21-induced Prdm1 gene regulation reveals functional cooperation of STAT3 and IRF4 transcription factors. Immunity. 2009; 31:941–952. [PubMed: 20064451]
11. Martins G, Calame K. Regulation and functions of Blimp-1 in T and B lymphocytes. Annu Rev Immunol. 2008; 26:133–169. [PubMed: 18370921]

12. Turner CAJ, Mack DH, Davis MM. Blimp-1, a novel zinc finger-containing protein that can drive the maturation of B lymphocytes into immunoglobulin-secreting cells. Cell. 1994; 77:297–306. [PubMed: 8168136]
13. Kallies A, et al. Plasma cell ontogeny defined by quantitative changes in Blimp-1 expression. J Exp Med. 2004; 200:967–977. [PubMed: 15492122]
14. Kallies A, et al. Initiation of plasma-cell differentiation is independent of the transcription factor Blimp-1. Immunity. 2007; 26:555–566. [PubMed: 17509907]
15. Shaffer AL, et al. Blimp-1 orchestrates plasma cell differentiation by extinguishing the mature B cell gene expression program. Immunity. 2002; 17:51–62. [PubMed: 12150891]
16. Su S-T, et al. Involvement of histone demethylase LSD1 in Blimp-1-mediated gene repression during plasma cell differentiation. Mol Cell Biol. 2009; 29:1421–1431. [PubMed: 19124609]
17. Györy I, Wu J, Fejér G, Seto E, Wright KL. PRDI-BF1 recruits the histone H3 methyltransferase G9a in transcriptional silencing. Nat Immunol. 2004; 5:299–308. [PubMed: 14985713]
18. Ren B, Chee KJ, Kim TH, Maniatis T. PRDI-BF1/Blimp-1 repression is mediated by corepressors of the Groucho family of proteins. Genes Dev. 1999; 13:125–137. [PubMed: 9887105]
19. Yu J, Angelin-Duclos C, Greenwood J, Liao J, Calame K. Transcriptional repression by Blimp-1 (PRDI-BF1) involves recruitment of histone deacetylase. Mol Cell Biol. 2000; 20:2592–2603. [PubMed: 10713181]
20. Lin Y, Wong K-K, Calame K. Repression of c-*myc* transcription by Blimp-1, an inducer of terminal B cell differentiation. Science. 1997; 276:596–599. [PubMed: 9110979]
21. Lin K-I, Angelin-Duclos C, Kuo TC, Calame K. Blimp-1-dependent repression of *Pax-5* is required for differentiation of B cells to immunoglobulin M-secreting plasma cells. Mol Cell Biol. 2002; 22:4771–4780. [PubMed: 12052884]
22. Piskurich JF, et al. BLIMP-1 mediates extinction of major histocompatibility class II transactivator expression in plasma cells. Nat Immunol. 2000; 1:526–532. [PubMed: 11101876]
23. Sciammas R, Davis MM. Modular nature of Blimp-1 in the regulation of gene expression during B cell maturation. J Immunol. 2004; 172:5427–5440. [PubMed: 15100284]
24. Kwon K, et al. Instructive role of the transcription factor E2A in early B lymphopoiesis and germinal center B cell development. Immunity. 2008; 28:751–762. [PubMed: 18538592]
25. Ohinata Y, et al. Blimp1 is a critical determinant of the germ cell lineage in mice. Nature. 2005; 436:207–213. [PubMed: 15937476]
26. Revilla-i-Domingo R, et al. The B-cell identity factor Pax5 regulates distinct transcriptional programmes in early and late B lymphopoiesis. EMBO J. 2012; 31:3130–3146. [PubMed: 22669466]
27. Jolma A, et al. DNA-binding specificities of human transcription factors. Cell. 2013; 152:327–339. [PubMed: 23332764]
28. Feil R, Wagner J, Metzger D, Chambon P. Regulation of Cre recombinase activity by mutated estrogen receptor ligand-binding domains. Biochem Biophys Res Commun. 1997; 237:752–757. [PubMed: 9299439]
29. Fooksman DR, et al. Development and migration of plasma cells in the mouse lymph node. Immunity. 2010; 33:118–127. [PubMed: 20619695]
30. Hargreaves DC, et al. A coordinated change in chemokine responsiveness guides plasma cell movements. J Exp Med. 2001; 194:45–56. [PubMed: 11435471]
31. Ochiai K, et al. Transcriptional regulation of germinal center B and plasma cell fates by dynamical control of IRF4. Immunity. 2013; 38:918–929. [PubMed: 23684984]
32. Yu Y, et al. Bcl11a is essential for lymphoid development and negatively regulates p53. J Exp Med. 2012; 209:2467–2483. [PubMed: 23230003]
33. Schulz D, et al. Gfi1b negatively regulates Rag expression directly and via the repression of FoxO1. J Exp Med. 2012; 209:187–199. [PubMed: 22201127]
34. Jackson JT, et al. A crucial role for the homeodomain transcription factor Hhex in lymphopoiesis. Blood. 2015; 125:803–814. [PubMed: 25472970]
35. Winkelmann R, et al. B cell homeostasis and plasma cell homing controlled by Krüppel-like factor 2. Proc Natl Acad Sci USA. 2011; 108:710–715. [PubMed: 21187409]

36. Martincic K, Alkan SA, Cheatle A, Borghesi L, Milcarek C. Transcription elongation factor ELL2 directs immunoglobulin secretion in plasma cells by stimulating altered RNA processing. Nat Immunol. 2009; 10:1102–1109. [PubMed: 19749764]
37. Benson MJ, et al. Heterogeneous nuclear ribonucleoprotein L-like (hnRNPLL) and elongation factor, RNA polymerase II, 2 (ELL2) are regulators of mRNA processing in plasma cells. Proc Natl Acad Sci USA. 2012; 109:16252–16257. [PubMed: 22991471]
38. Park KS, et al. Transcription elongation factor ELL2 drives Ig secretory-specific mRNA production and the unfolded protein response. J Immunol. 2014; 193:4663–4674. [PubMed: 25238757]
39. Kong SE, Banks CA, Shilatifard A, Conaway JW, Conaway RC. ELL-associated factors 1 and 2 are positive regulators of RNA polymerase II elongation factor ELL. Proc Natl Acad Sci USA. 2005; 102:10094–10098. [PubMed: 16006523]
40. Vincent-Fabert C, et al. Genomic deletion of the whole IgH 3' regulatory region (hs3a, hs1,2, hs3b, and hs4) dramatically affects class switch recombination and Ig secretion to all isotypes. Blood. 2010; 116:1895–1898. [PubMed: 20538806]
41. Buenrostro JD, Giresi PG, Zaba LC, Chang HY, Greenleaf WJ. Transposition of native chromatin for fast and sensitive epigenomic profiling of open chromatin, DNA-binding proteins and nucleosome position. Nat Methods. 2013; 10:1213–1218. [PubMed: 24097267]
42. Margueron R, Reinberg D. The Polycomb complex PRC2 and its mark in life. Nature. 2011; 469:343–349. [PubMed: 21248841]
43. Klose RJ, Cooper S, Farcas AM, Blackledge NP, Brockdorff N. Chromatin sampling – an emerging perspective on targeting polycomb repressor proteins. PLoS Genet. 2013; 9 e1003717.
44. Illingworth RS, et al. Orphan CpG islands identify numerous conserved promoters in the mammalian genome. PLoS Genet. 2010; 6 e1001134.
45. Ho L, Crabtree GR. Chromatin remodelling during development. Nature. 2010; 463:474–484. [PubMed: 20110991]
46. Perissi V, Jepsen K, Glass CK, Rosenfeld MG. Deconstructing repression: evolving models of co-repressor action. Nat Rev Genet. 2010; 11:109–123. [PubMed: 20084085]
47. Nettles KW, Greene GL. Ligand control of coregulator recruitment to nuclear receptors. Annu Rev Physiol. 2005; 67:309–333. [PubMed: 15709961]
48. Anelli T, et al. Sequential steps and checkpoints in the early exocytic compartment during secretory IgM biogenesis. EMBO J. 2007; 26:4177–4188. [PubMed: 17805346]
49. Rosenbaum M, et al. MZB1 is a GRP94 cochaperone that enables proper immunoglobulin heavy chain biosynthesis upon ER stress. Genes Dev. 2014; 28:1165–1178. [PubMed: 24888588]
50. Manis JP, et al. Class switching in B cells lacking 3' immunoglobulin heavy chain enhancers. J Exp Med. 1998; 188:1421–1431. [PubMed: 9782119]
51. Li P, et al. BATF-JUN is critical for IRF4-mediated transcription in T cells. Nature. 2012; 490:543–546. [PubMed: 22992523]
52. Cobaleda C, Jochum W, Busslinger M. Conversion of mature B cells into T cells by dedifferentation to uncommitted progenitors. Nature. 2007; 449:473–477. [PubMed: 17851532]

Online Methods References

1. Ohinata Y, et al. Blimp1 is a critical determinant of the germ cell lineage in mice. Nature. 2005; 436:207–213. [PubMed: 15937476]
2. Kallies A, et al. Plasma cell ontogeny defined by quantitative changes in Blimp-1 expression. J Exp Med. 2004; 200:967–977. [PubMed: 15492122]
3. Tallquist MD, Soriano P. Epiblast-restricted Cre expression in MORE mice: a tool to distinguish embryonic vs. extra-embryonic gene function. Genesis. 2000; 26:113–115. [PubMed: 10686601]
4. Rodriguez CI, et al. High-efficiency deleter mice show that FLPe is an alternative to Cre-*loxP*. Nat Genet. 2000; 25:139–140. [PubMed: 10835623]
5. Kwon K, et al. Instructive role of the transcription factor E2A in early B lymphopoiesis and germinal center B cell development. Immunity. 2008; 28:751–762. [PubMed: 18538592]

6. de Boer E, et al. Efficient biotinylation and single-step purification of tagged transcription factors in mammalian cells and transgenic mice. Proc Natl Acad Sci USA. 2003; 100:7480–7485. [PubMed: 12802011]
7. Smith KG, Light A, Nossal GJ, Tarlinton DM. The extent of affinity maturation differs between the memory and antibody-forming cell compartments in the primary immune response. EMBO J. 1997; 16:2996–3006. [PubMed: 9214617]
8. Dörfler P, Busslinger M. C-terminal activating and inhibitory domains determine the transactivation potential of BSAP (Pax-5), Pax-2 and Pax-8. EMBO J. 1996; 15:1971–1982. [PubMed: 8617244]
9. Feil R, Wagner J, Metzger D, Chambon P. Regulation of Cre recombinase activity by mutated estrogen receptor ligand-binding domains. Biochem Biophys Res Commun. 237:752–757.
10. Heavey B, Charalambous C, Cobaleda C, Busslinger M. Myeloid lineage switch of *Pax5* mutant but not wild-type B cell progenitors by C/EBPα and GATA factors. EMBO J. 2003; 22:3887–3897. [PubMed: 12881423]
11. Dyer RB, Herzog NK. Isolation of intact nuclei for nuclear extract preparation from a fragile B-lymphocyte cell line. BioTechniques. 1995; 19:192–195. [PubMed: 8527134]
12. Buenrostro JD, Giresi PG, Zaba LC, Chang HY, Greenleaf WJ. Transposition of native chromatin for fast and sensitive epigenomic profiling of open chromatin, DNA-binding proteins and nucleosome position. Nat Methods. 2013; 10:1213–1218. [PubMed: 24097267]
13. Schebesta A, et al. Transcription factor Pax5 activates the chromatin of key genes involved in B cell signaling, adhesion, migration, and immune function. Immunity. 2007; 27:49–63. [PubMed: 17658281]
14. Ebert A, et al. The distal V_H gene cluster of the *Igh* locus contains distinct regulatory elements with Pax5 transcription factor-dependent activity in pro-B cells. Immunity. 2011; 34:175–187. [PubMed: 21349430]
15. Parkhomchuk D, et al. Transcriptome analysis by strand-specific sequencing of complementary DNA. Nucleic Acids Res. 2009; 37:e123. [PubMed: 19620212]
16. Zhang Y, et al. Model-based analysis of ChIP-Seq (MACS). Genome Biol. 2008; 9:R137. [PubMed: 18798982]
17. Revilla-i-Domingo R, et al. The B-cell identity factor Pax5 regulates distinct transcriptional programmes in early and late B lymphopoiesis. EMBO J. 2012; 31:3130–3146. [PubMed: 22669466]
18. Zang C, et al. A clustering approach for identification of enriched domains from histone modification ChIP-Seq data. Bioinformatics. 2009; 25:1952–1958. [PubMed: 19505939]
19. Narlikar L, Jothi R. ChIP-Seq data analysis: identification of protein-DNA binding sites with SISSRs peak-finder. Methods Mol Biol. 2012; 802:305–322. [PubMed: 22130889]
20. Machanick P, Bailey TL. MEME-ChIP: motif analysis of large DNA datasets. Bioinformatics. 2011; 27:1696–1697. [PubMed: 21486936]
21. Katoh K, Misawa K, Kuma K, Miyata T. MAFFT: a novel method for rapid multiple sequence alignment based on fast Fourier transform. Nucleic Acids Res. 2002; 30:3059–3066. [PubMed: 12136088]
22. Crooks GE, Hon G, Chandonia JM, Brenner SE. WebLogo: a sequence logo generator. Genome Res. 2004; 14
23. Aszódi A. MULTOVL: fast multiple overlaps of genomic regions. Bioinformatics. 2012; 28:3318–3319. [PubMed: 23071271]
24. Micallef L, Rodgers P. eulerAPE: drawing area-proportional 3-Venn diagrams using ellipses. PLoS One. 2014; 9 e101717.
25. Illingworth RS, et al. Orphan CpG islands identify numerous conserved promoters in the mammalian genome. PLoS Genet. 2010; 6 e1001134.
26. Long HK, et al. Epigenetic conservation at gene regulatory elements revealed by non-methylated DNA profiling in seven vertebrates. eLife. 2013; 2 e00348.
27. Trapnell C, Pachter L, Salzberg SL. TopHat: discovering splice junctions with RNA-Seq. Bioinformatics. 2009; 25:1105–1111. [PubMed: 19289445]

28. Anders S, Pyl PT, Huber W. HTSeq–a Python framework to work with high-throughput sequencing data. Bioinformatics. 2015; 31:166–169. [PubMed: 25260700]
29. Risso D, Schwartz K, Sherlock G, Dudoit S. GC-content normalization for RNA-Seq data. BMC bioinformatics. 2011; 12:480. [PubMed: 22177264]
30. Anders S, Huber W. Differential expression analysis for sequence count data. Genome Biol. 2010; 11:R106. [PubMed: 20979621]
31. Cunningham F, et al. Ensembl 2015. Nucleic Acids Res. 2015; 43:D662–D669. [PubMed: 25352552]

Europe PMC Funders Author Manuscripts

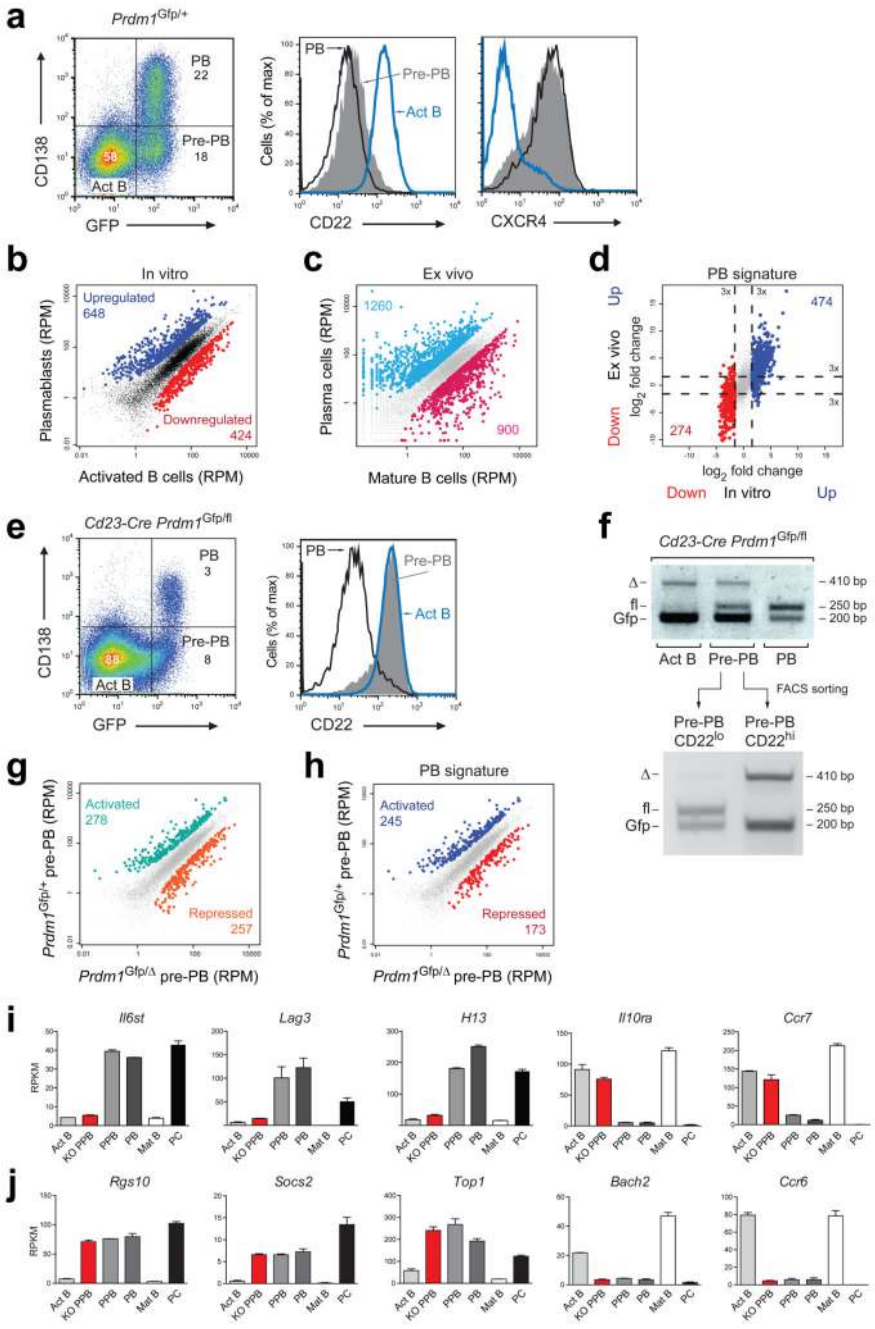

Figure 1. Blimp1-dependent gene expression changes during plasma cell differentiation.

(**a**) In vitro plasmablast differentiation. B220^{+} B cells from spleen and lymph nodes of *Prdm1*$^{Gfp/+}$ mice were stimulated with LPS for 4 days prior to flow cytometric analysis of activated B cells (Act B; CD138^{-}GFP^{-}), pre-plasmablasts (pre-PB; CD138^{-}GFP^{+}) and plasmablasts (PB; CD138^{+}GFP^{+}). Numbers refer to the percent of cells in the indicated gates. Cell surface expression of CD22 and CXCR4 on the three cell types is shown to the right. (**b**) Scatter plot of gene expression differences between in vitro differentiated activated B cells and plasmablasts of the *Prdm1*$^{Gfp/+}$ genotype, based on two independent RNA-seq

experiments for each cell type. The normalized expression data of individual genes in the two cell types were plotted as RPM values. Each symbol represents one gene. Genes with an expression difference of > 3-fold, an adjusted *P* value of < 0.1 and an RPKM value of > 3 in plasmablasts (up-regulated) or activated B cells (down-regulated) are colored in blue or red, corresponding to up- or down-regulated genes in plasmablasts, respectively. For evaluation of the RNA-seq data, see Online Methods. (**c**) Gene expression differences between ex vivo sorted *Prdm1*$^{Gfp/+}$ plasma cells (B220^{lo}CD28^{+}CD138^{+}GFP^{+}Lin^{-}) from the bone marrow and wild-type mature B cells (B220^{+}CD19^{+}IgD^{hi}) from lymph nodes. The RNA-seq data were analyzed with the same cutoffs as described in **b**. Two independent RNA-seq experiments were performed for each cell type. (**d**) Overlap of the gene expression signatures between in vivo bone marrow plasma cells and in vitro differentiated plasmablasts. The $\log_2$ fold expression change observed between in vitro differentiated activated B cells and plasmablasts (x-axis) as well as between ex vivo sorted mature B cells and plasma cells (y-axis) is plotted for each gene. The 648 up-regulated (Up) and 424 down-regulated (Down) genes identified in the activated B cell-to-plasmablast transition (plasmablast signature; **b**) are indicated as blue and red dots, respectively. (**e**) In vitro differentiation of mature B cells from the spleen and lymph nodes of *Cd23*-Cre *Prdm1*$^{Gfp/fl}$ mice with LPS for 4 days prior to flow cytometric analysis as described in **a**. (**f**) PCR genotyping of FACS-sorted activated B cells (Act B; CD138^{-}GFP^{-}), pre-plasmablasts (pre-PB; CD138^{-}GFP^{+}, top row) and plasmablasts (PB; CD138^{+}GFP^{+}). The pre-plasmablasts were further separated into CD22^{lo}CD138^{-}GFP^{+} and CD22^{hi}CD138^{-}GFP^{+} cells (bottom row). The positions of the PCR fragments corresponding to the *Gfp*-tagged, intact floxed (fl) and deleted (Δ) *Prdm1* alleles are shown to the left, and their size is indicated in base pairs (bp) to the right. (**g**) Scatter plot of gene expression differences between experimental *Prdm1*$^{Gfp/\Delta}$ and control *Prdm1*$^{Gfp/+}$ pre-plasmablasts, based on two independent RNA-seq experiments for each cell type, as described in **b**. (**h)** Overlap of Blimp1-regulated genes with the plasmablast signature. Genes, which correspond to up-regulated (blue) or down-regulated (red) genes identified in the B cell-to-plasmablast transition (plasmablast signature; **b**), are indicated in the scatter plot of gene expression differences between *Prdm1*$^{Gfp/\Delta}$ and *Prdm1*$^{Gfp/+}$ pre-plasmablasts. Numbers refer to Blimp1-regulated genes, which are > 3 fold up- or down-regulated in the plasmablast transition. (**i**) Expression of Blimp1-dependent cell surface receptor genes during LPS-induced plasmablast differentiation and in ex vivo sorted mature B cells (Mat B) and plasma cells (PC). The expression of each gene is shown as normalized gene-expression RPKM value with SEM, based on two RNA-seq experiments for each cell type. PPB, pre-plasmablasts; KO PPB, *Prdm1*$^{Gfp/\Delta}$PPB. (**j**) Expression of Blimp1-independent genes during LPS-induced plasmablast differentiation as well as in mature B and plasma cells. Blimp1-independent genes were defined by a < 1.6-fold expression difference between *Prdm1*$^{Gfp/\Delta}$ and control *Prdm1*$^{Gfp/+}$ pre-plasmablasts (shown in grey in **h**). RPM, reads per gene per million mapped sequence reads; RPKM, reads per kilobase of exon per million mapped sequence reads.

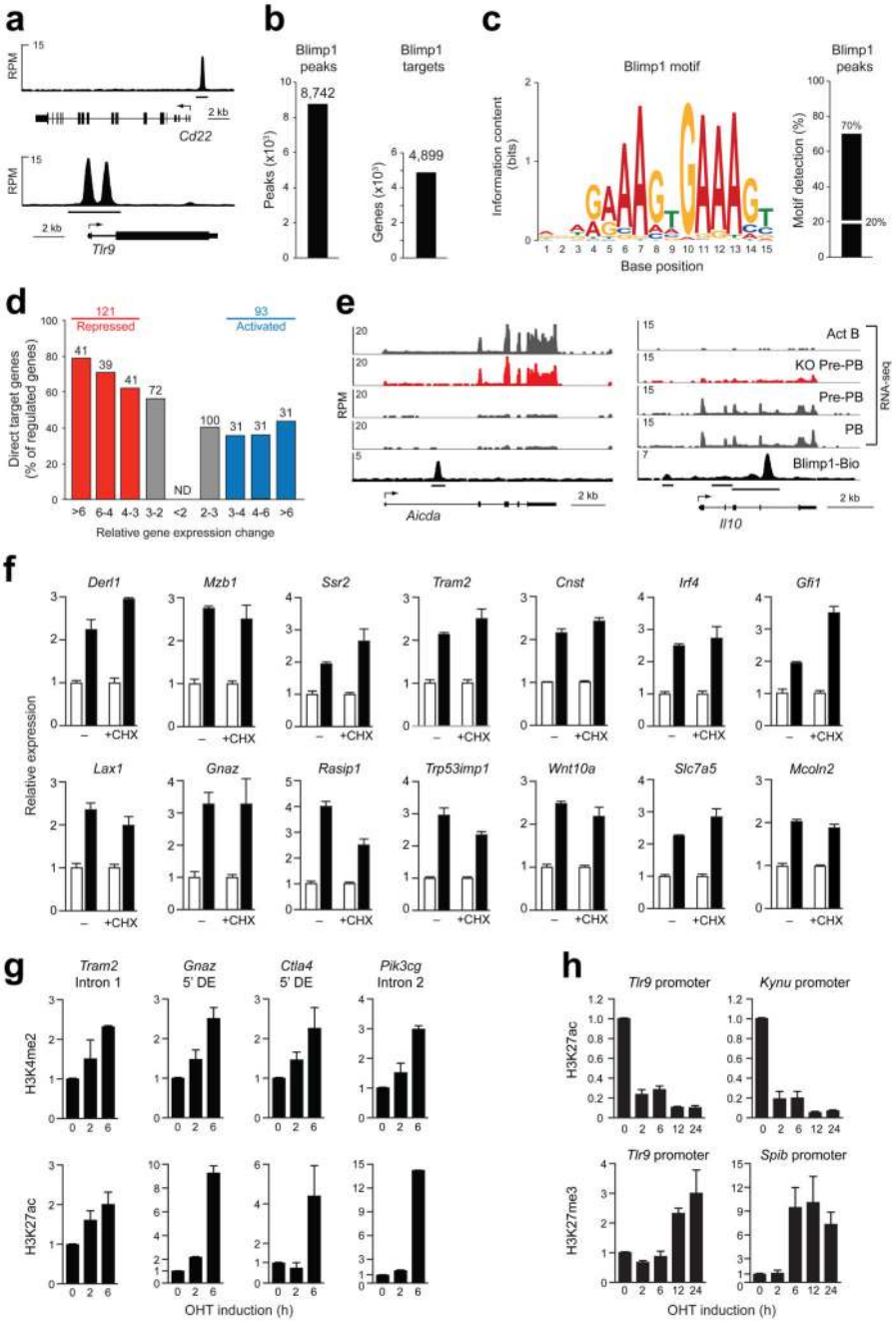

Figure 2. Identification of regulated Blimp1 target genes.

(**a**) Blimp1 binding at the *Cd22* and *Tlr9* genes in plasmablasts. B220^{+} mature B cells from the spleen and lymph nodes of *Prdm1*$^{Bio/Bio}$ *Rosa26*$^{BirA/BirA}$ mice were stimulated for 4 days with LPS prior to Bio-ChIP-sequencing26. Blimp1 peaks are shown together with the exon-intron structure of the gene and a scale bar shown in kilobases (kb). Bars below the ChIP-seq track indicate Blimp1-binding regions identified by MACS peak calling. (**b**) Identification of 8,742 Blimp1 peaks in plasmablasts with a stringent *P* value of $< 10^{-10}$, as determined by MACS peak calling. Peak-to-gene assignment26 identified 4,899 Blimp1

Europe PMC Funders Author Manuscripts

target genes in plasmablasts. (**c**) Consensus Blimp1 recognition sequence identified by the de novo motif discovery program MEME-ChIP. The Blimp1-binding motif with an E-value of $3x10^{-356}$ was detected at 70% of all Blimp1 peaks in plasmablasts (right). The same motif was found in random DNA sequences at a frequency of 20% (indicated by a white line). (**d**) Identification of activated and repressed Blimp1 target genes in pre-plasmablasts. The number and percentage of Blimp1 target genes are shown for the indicated fold gene expression differences between experimental *Prdm1*$^{Gfp/\Delta}$ and control *Prdm1*$^{Gfp/+}$ pre-plasmablasts, as defined in Fig. 1h. Activated and repressed genes were selected for an RPKM value of > 3 in control *Prdm1*$^{Gfp/+}$ pre-plasmablasts (activated) or experimental *Prdm1*$^{Gfp/\Delta}$ pre-plasmablasts (repressed), respectively. ND, not determined. (**e**) Expression of the regulated Blimp1 target genes *Aicda* and *Il10* in *Prdm1*$^{Gfp/\Delta}$ (KO) pre-plasmablasts and activated B cells, pre-plasmablasts and plasmablasts of the control *Prdm1*$^{Gfp/+}$ genotype, as shown by RNA-seq analysis. Blimp1 peaks were identified in plasmablasts by Bio-ChIP-seq, as described in **a**. (**f**) Direct activation of target genes by Blimp1-ER^{T2} in the absence of protein synthesis. Where indicated, the WEHI-231 B cells expressing the Blimp1-estrogen receptor (ER^{T2}) fusion protein were pre-incubated with cycloheximide (CHX; 25 μg/ml) for 30 min prior to the addition of 4-hydroxytamoxifen (OHT; 1 μM) for 6 h, which was followed by RNA isolation and RT-qPCR analysis of nascent transcripts of the indicated genes, as described in the Online Methods. The transcript value of each gene was normalized to the corresponding value of the *Tbp* gene coding for the TATA box-binding protein. The normalized value was set to 1 for the cells that were not treated with OHT. Average values with SEM are shown for three independent experiments. No PCR signal was observed, if the reverse transcriptase was omitted. (**g**) Induction of active chromatin at Blimp1-binding sites of activated target genes. WEHI-Blimp1-ER^{T2} cells were treated with OHT (1 μM) for up to 6 h prior to ChIP analysis with H3K4me2- or H3K27ac-specific antibodies. Input and precipitated DNA were quantified by real-time PCR with primer pairs amplifying the Blimp1-binding regions of the indicated genes and the promoter of the ubiquitously expressed control *Tbp* gene. The amount of precipitated DNA was determined as percentage relative to input DNA for each region analyzed and is shown as relative enrichment at the target site compared to the *Tbp* promoter by dividing the percentage of precipitated DNA at the Blimp1-binding site (target ChIP/target input) by the percentage of precipitated DNA at the *Tbp* promoter (*Tbp* ChIP/*Tbp* input). The normalized value was set to 1 for the time point 0. Average values with SEM are shown for two independent experiments. DE, distal element. (**h**) Abundance of the active H3K27ac and repressive H3K27me3 histone marks at Blimp1-binding sites of repressed target genes in OHT-stimulated WEHI-Blimp1-ER^{T2} cells. The data of two independent ChIP experiments were evaluated and normalized as described in **g**.

Europe PMC Funders Author Manuscripts

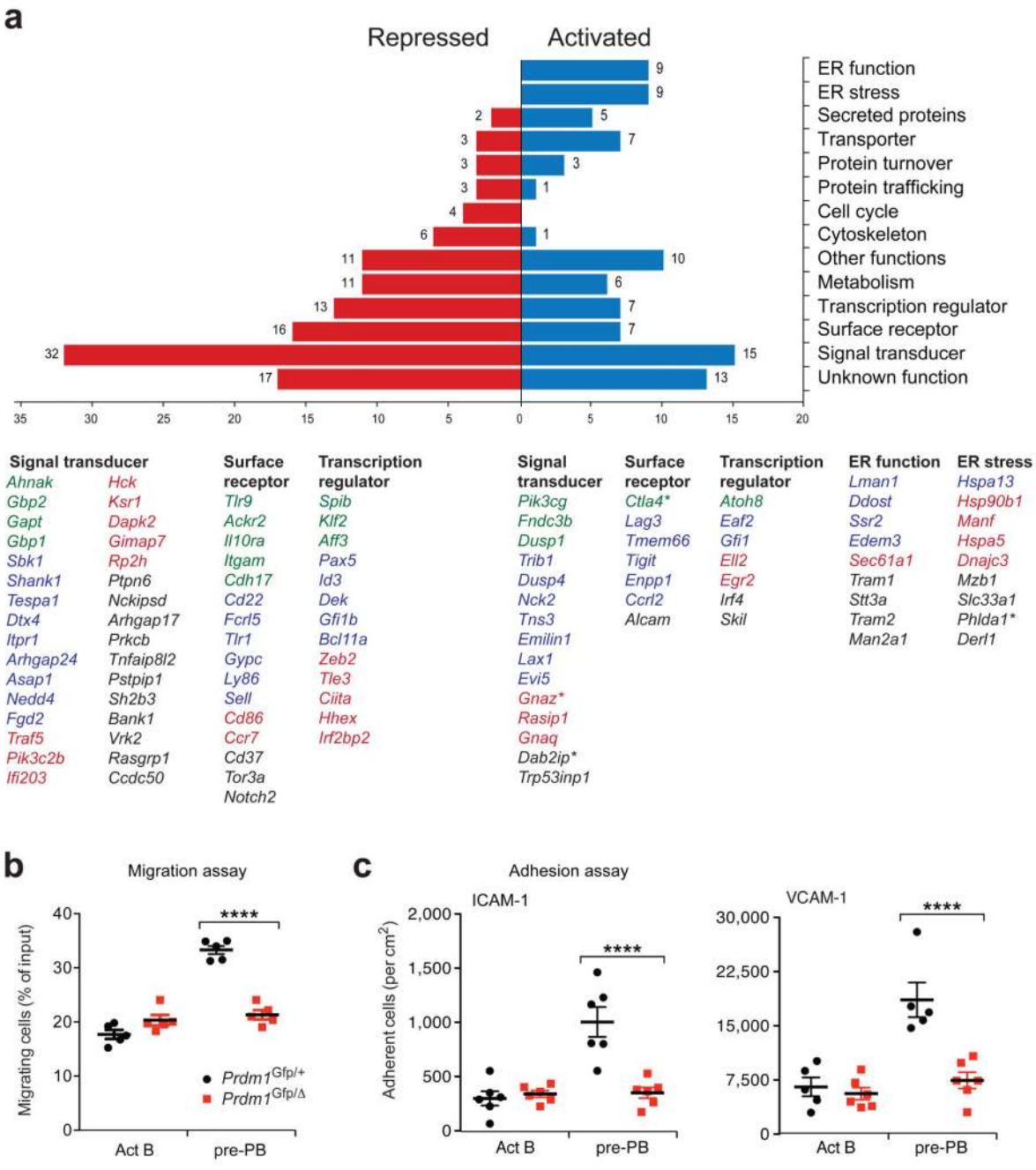

Figure 3. Function of activated and repressed Blimp1 target genes in plasmablasts.

(**a**) Functional classification and quantification (numbers) of the proteins encoded by activated and repressed Blimp1 target genes in pre-plasmablasts. Regulated Blimp1 target genes of selected functional classes are shown below and ranked according to their fold expression changes observed between *Prdm1*$^{Gfp/\Delta}$ and *Prdm1*$^{Gfp/+}$ pre-plasmablasts (Fig. 2d). The color code refers to >10-fold (green), 5-10-fold (blue), 4-5-fold (red) and 3-4-fold (black). Genes with low expression in bone marrow plasma cells compared to LPS-stimulated plasmablasts are indicated by an asterisk. (**b**) Transwell migration assay. LPS-

stimulated activated B cells (Act B) and pre-plasmablasts of the indicated genotypes in IMDM medium were placed in the upper compartment, whereas IMDM medium containing 400 ng/ml CXCL12 (SDF-1α) was present in the lower compartment of a transwell chamber separated by a filter of 5 μm-pore size. Cells migrating into the lower chamber after a 2-hour incubation at 37°C were measured in a Casy cell counter and are indicated as percentage of the total cells per well. The average percentage and SEM of one of four independent experiments are shown. Each symbol represents the cell count of one well. (**c**) Adhesion assay. LPS-stimulated activated B cells and pre-plasmablasts of the indicated genotypes were allowed to adhere to ICAM1-Fc- or VCAM1-Fc-coated glass slides in the presence of CXCL12 for 6 hours in DMEM medium, washed 2 times and fixed in 4% paraformaldehyde (see Online Methods). Individual wells (represented by symbols) were evaluated by automatic cell counting, and the average cell density with SEM is shown for one of four (ICAM-1) or two (VCAM-1) independent experiments. Each symbol represents the result of one well. **** $P < 0.0001$ (two-way analysis of variance (ANOVA) with Bonferroni's post-test).

Europe PMC Funders Author Manuscripts

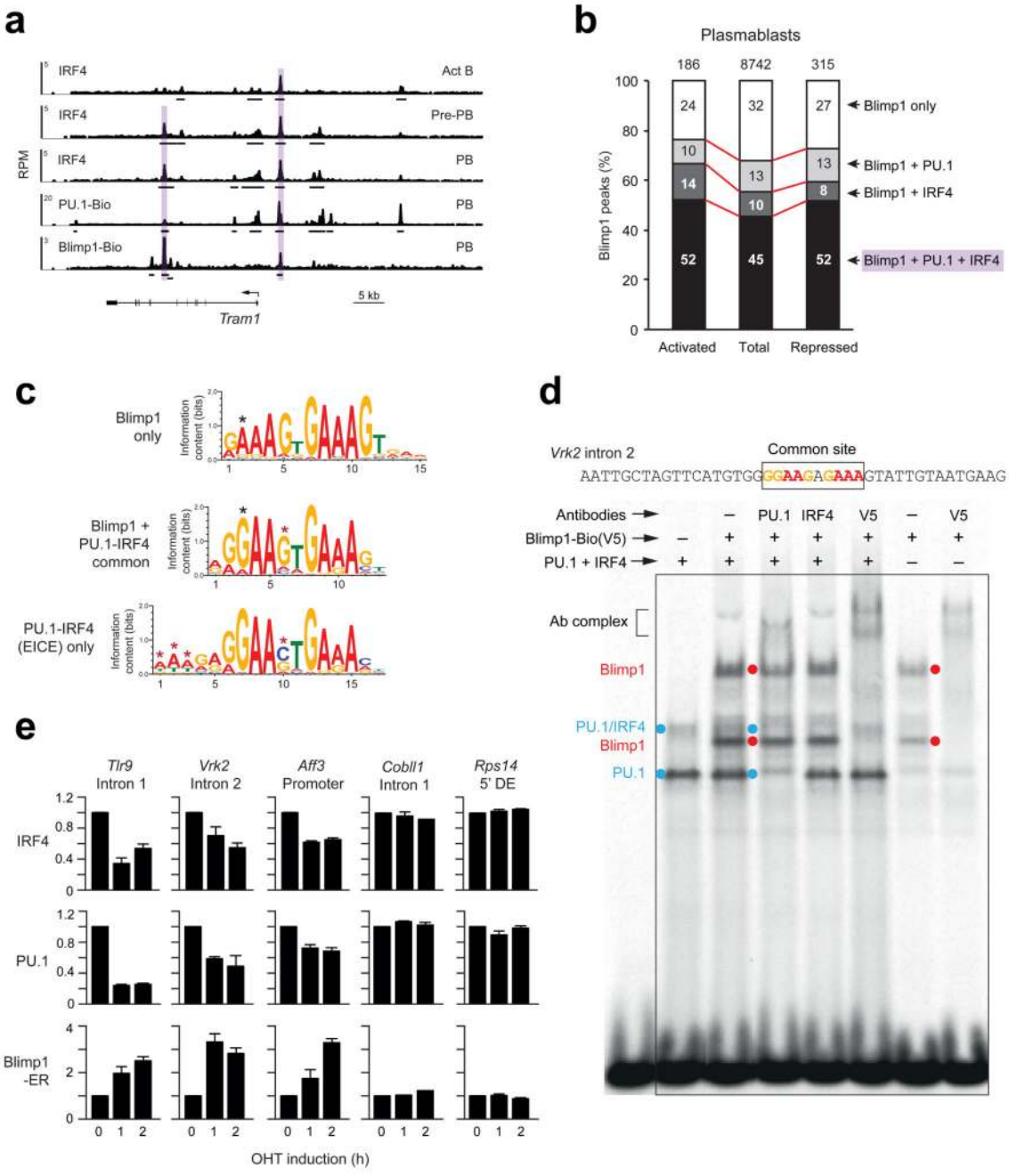

Figure 4. Mutually exclusive binding of Blimp1 and the PU.1-IRF4 complex to a common recognition motif in plasmablasts.

(**a**) Binding patterns of IRF4, PU.1 and Blimp1 in CD138^{+} plasmablasts at day 4 of LPS stimulation. The binding of IRF4 was analyzed by ChIP-seq with an IRF4 antibody, whereas PU.1 (*Spi1*) binding was determined by Bio-ChIP-seq of plasmablasts from *Spi1*$^{Bio/Bio}$ *Rosa26*$^{BirA/BirA}$ mice (**Supplementary Fig. 4d**). IRF4 and PU.1 peaks were called with a stringent *P* value of 10^{-10}. (**b**) Colocalization of Blimp1 peaks with binding sites of IRF4 and PU.1 in plasmablasts, as determined by multiple overlap analysis of the respective ChIP-

Europe PMC Funders Author Manuscripts

seq data. The overlap of binding sites is shown as percentage relative to the total Blimp1-binding sites (Fig. 2b) or Blimp1-binding sites present at activated and repressed Blimp1 target genes (Fig. 2d). (**c**) Consensus motif of the common binding sites for Blimp1 and the PU.1-IRF4 complex (middle). The common binding sites were bioinformatically identified by the strict colocalization of the Blimp1-binding and EICE motifs in the 3,806 peaks characterized by overlapping Blimp1, IRF4 and PU.1 binding (Supplementary Fig. 4a). For comparison, the Blimp1-only and EICE motifs (Supplementary Fig. 4a) are shown together with their deviation from the common motif, which is indicated by black (Blimp1-only) and red (EICE) asterisks. (**d**) Mutually exclusive binding of Blimp1 and the PU.1-IRF4 complex to a common binding site present in the second intron of the repressed Blimp1 target gene *Vrk2*. The Blimp1-Bio (V5), IRF4 and PU.1 proteins were individually expressed in transfected HEK-293T cells and analyzed by electromobility shift assay (EMSA) for binding to the common binding site probe of the *Vrk2* gene. Anti-PU.1, anti-IRF4 and anti-V5 antibody (Ab) were added to the binding reaction, where indicated. The different protein-DNA and Ab complexes are indicated. (**e**) Displacement of IRF4 and PU.1 from common binding sites by Blimp1-ER. WEHI-Blimp1-ER^{T2} B cells were treated with OHT (1 μM) for 1 or 2 h prior to ChIP analysis with anti-IRF4, anti-PU.1 or anti-ER antibodies. Input and precipitated DNA were quantified by real-time PCR with primer pairs amplifying the common-binding regions of the indicated genes shown in Supplementary Fig. 4c. The amount of precipitated DNA was determined as percentage relative to input DNA for each region analyzed, and the relative enrichment was set to 1 for the time point 0. Average values with SEM are shown for three independent experiments. DE, distal element.

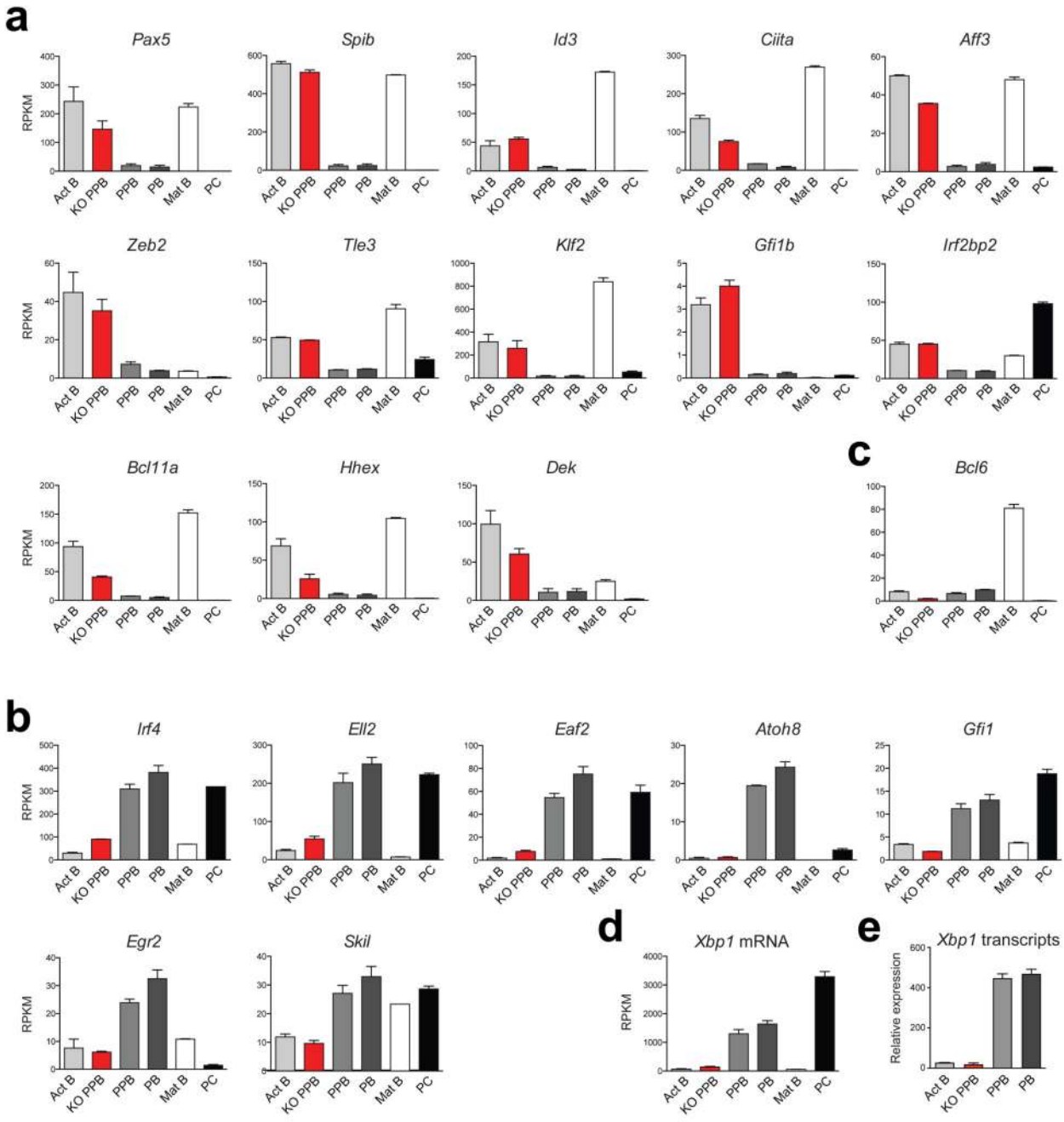

Figure 5. Blimp1-dependent regulation of transcription factor genes in plasmablasts.

(**a**,**b**) Expression of the repressed (**a**) and activated (**b**) Blimp1 target genes coding for transcriptional regulators. The expression of the indicated genes was determined by RNA-sequencing of LPS-stimulated *Prdm1*$^{Gfp/\Delta}$ pre-plasmablasts (KO PPB, red) and activated B cells (Act B, light grey), pre-plasmablasts (PPB, grey) and plasmablasts (PB, dark grey) of the control *Prdm1*$^{Gfp/+}$ genotype as well as ex vivo sorted wild-type lymph node B cells (Mat B, white) and bone marrow plasma cells (PC, black). Gene expression is shown as normalized expression value (RPKM) with SEM, based on two independent RNA-seq

Europe PMC Funders Author Manuscripts

experiments for each cell type. (**c**,**d**) Expression of *Bcl6* (**c**) and the Blimp1-activated *Xbp1* gene (**d**) during plasma cell differentiation. (**e**) RT-qPCR analysis of nascent *Xbp1* transcripts in the indicated cell types. The amount of nascent *Xbp1* transcripts (intron 2) was normalized to the amount of nascent *Tbp* transcripts (intron 1).

Europe PMC Funders Author Manuscripts

Europe PMC Funders Author Manuscripts

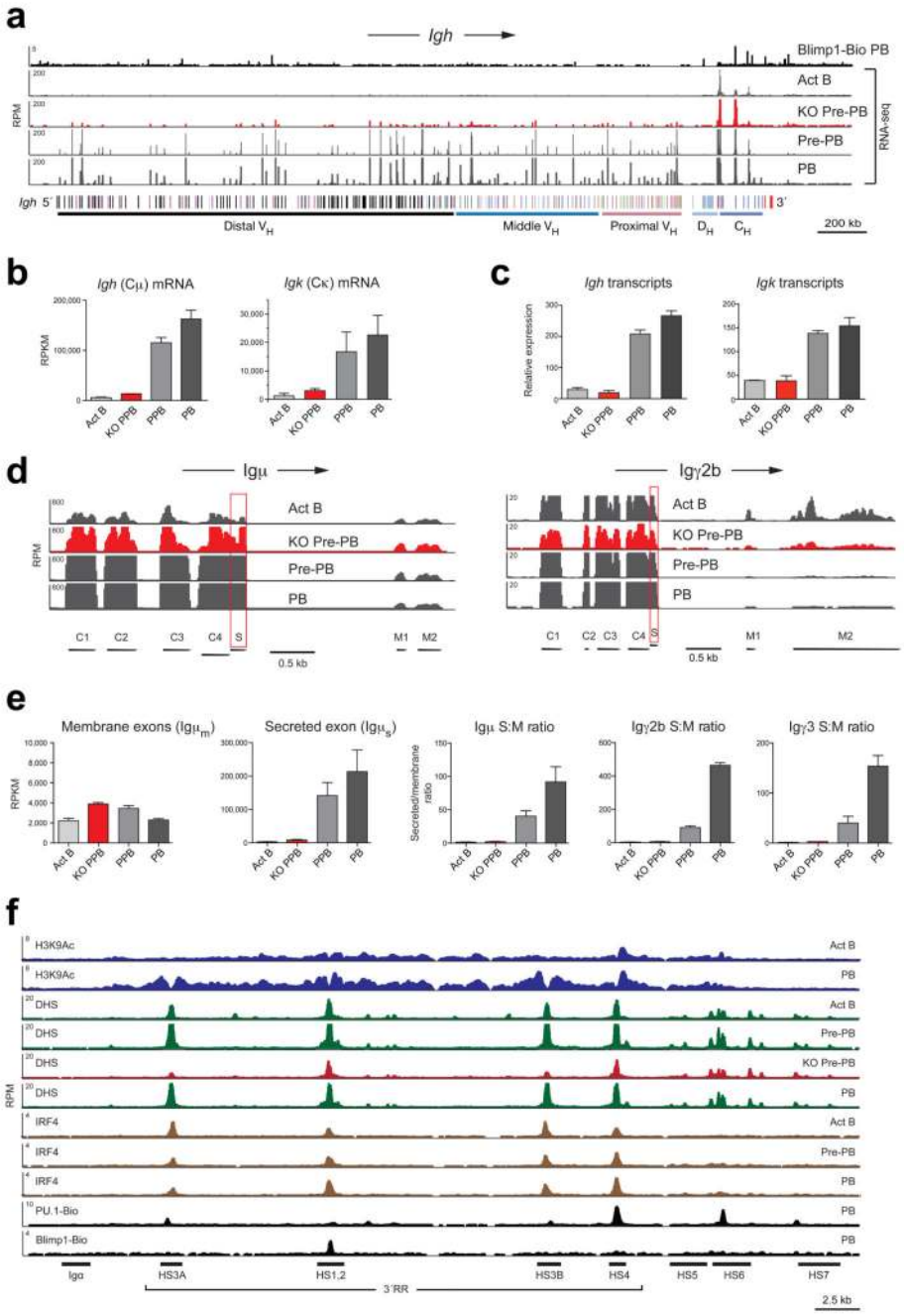

Figure 6. Blimp1-dependent activation of immunoglobulin gene transcription in plasmablasts.

(**a**) Blimp1 binding and transcript abundance at the *Igh* locus. The binding of the Blimp1-Bio protein (determined by ChIP-seq; top row) in plasmablasts (PB) and the abundance of the *Igh* gene transcripts (determined by RNA-seq) are shown for LPS-stimulated *Prdm1*$^{Gfp/\Delta}$ pre-plasmablasts (KO Pre-PB, red) as well as for activated B cells (Act B, light grey), pre-plasmablasts (Pre-PB, grey) and plasmablasts (PB, black) of the control *Prdm1*$^{Gfp/+}$ genotype. The annotation of the C57BL/6 *Igh* locus (below) indicates the distinct V_H gene families (different colors) in the distal, middle and proximal V_H gene regions as well as the

D_H (grey), C_H (blue) elements and Eμ and 3'RR enhancers (red) in the 3' proximal *Igh* domain. (**b**) Normalized expression (RPKM) of the Igμ and *Igk* constant exons in the indicated cell types. (**c)** RT-qPCR analysis of nascent *Igh* and *Igk* transcripts in the indicated cell types. The amount of nascent transcripts of the rearranged *Igh* (Igμ intron 2) and *Igk* (intron 1) genes was normalized to the amount of nascent *Tbp* transcripts (intron 1). (**d**) RNA abundance at the Igμ and Igγ2b genes, as described in **a**. (**e**) The RPKM expression values for the membrane ($Ig\mu_m$) and secreted ($Ig\mu_s$) exons are shown for the different cell types together with the $Ig\mu_s$ / $Ig\mu_m$, $Ig\gamma2b_s$ / $Ig\gamma2b_m$ and $Ig\gamma3_s$ / $Ig\gamma3_m$ mRNA ratios (S:M). (**f**) Chromatin changes and transcription factor binding at the 3' regulatory region (3'RR) of the *Igh* locus during the transition from activated B cells to plasmablasts. DHS sites were determined by ATAC-seq, the active histone mark H3K9ac and IRF4 binding by ChIP-seq and the binding of PU.1-Bio and Blimp1-Bio by Bio-ChIP-seq. The enhancers (HS3A, HS1/2, HS3B, HS4) of the 3' RR are shown below together with the 3' CTCF-binding element (3'CBE) region (HS5, HS6, HS7).

Europe PMC Funders Author Manuscripts

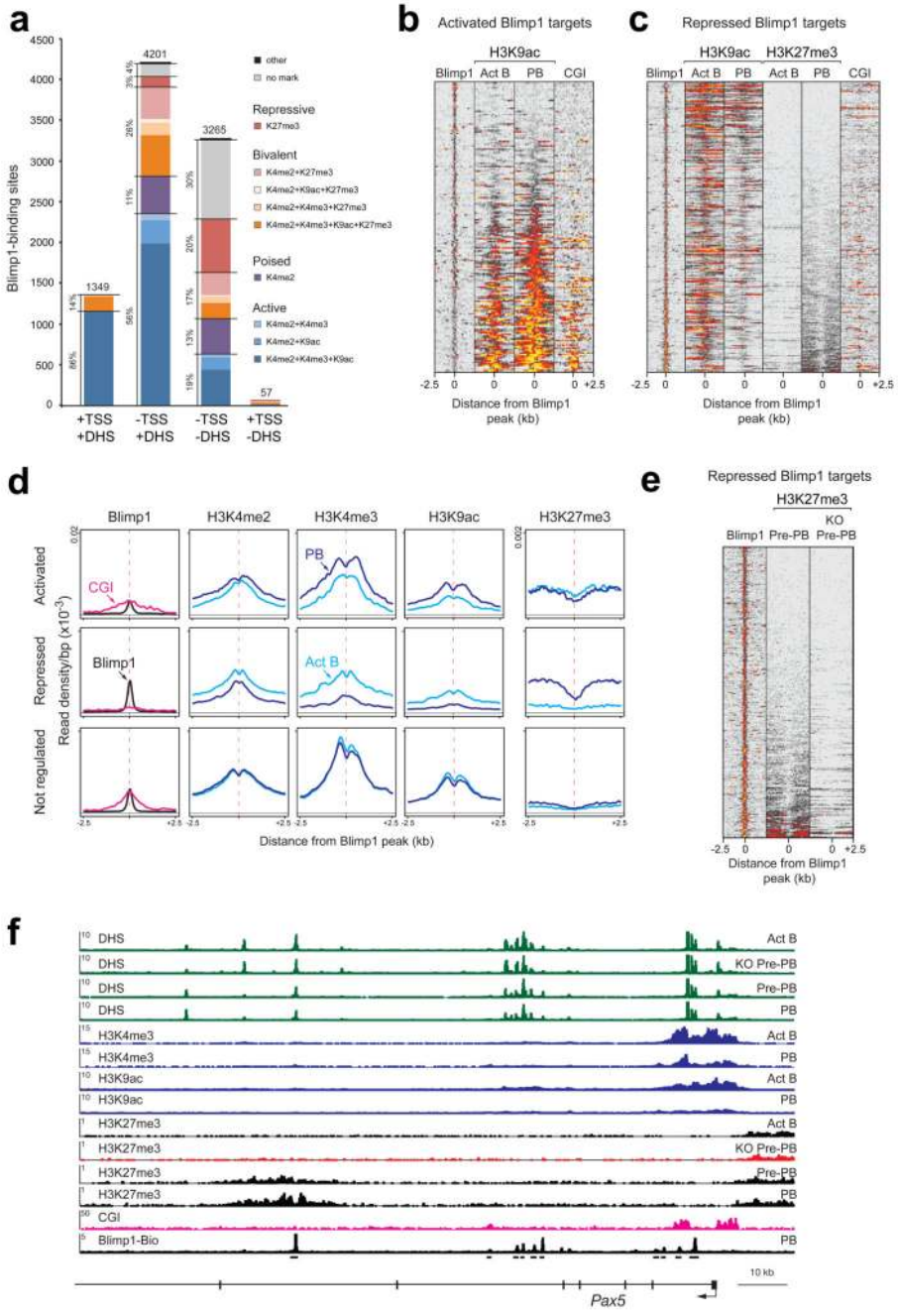

Figure 7. Chromatin changes at regulated Blimp1 target genes in plasmablasts.

(**a**) Overlap of Blimp1-binding sites with the regulatory landscape of plasmablasts. 'Active' promoters were defined by DHS sites (identified by ATAC-seq) overlapping with an mm9-annotated transcription start site (TSS). 'Active' distal elements were identified by the presence of a DHS site lacking a TSS. Regions of active, poised, bivalent and repressive chromatin were defined by the indicated combinations of active (H3K4me2, H3K4me3, H3K9ac) and repressive (H3K27me3) histone modifications, which were determined by ChIP-seq analysis in plasmablasts (Supplementary Fig. 7b). (**b**,**c**) Presence of H3K9ac or

H3K27me3 in activated B cells (Act B) and plasmablasts (PB) at Blimp1-binding sites of activated (**b**) or repressed (**c**) target genes, respectively. The densities of Blimp1 binding, H3K9ac, H3K27me3 and CpG islands (CGI, blood)44 are displayed as heat maps that are shown for a region extending from -2.5 kb to +2.5 kb relative to the Blimp1 peak summit and were sorted according to the increasing density of H3K9ac (**b**) or H3K27me3 (**c**) in plasmablasts. Density scale; low (grey), intermediate (red), high (yellow). (**d**) The average density of Blimp1-binding (black, plasmablasts) and CpG islands (CGI; red, blood cells) as well as of the indicated histone marks in activated B cells (light blue) and plasmablasts (dark blue) are shown for a region extending from -2.5 kb to +2.5 kb relative to the Blimp1-binding sites present of activated (>3x), repressed (>3x) and not regulated (1-1.25x) Blimp1 target genes. (**e**) Absence of H3K27me3 at repressed Blimp1 target genes in Blimp1-deficient pre-plasmablasts. H3K27me3 was mapped by ChIP-seq analysis of *Prdm1*$^{Gfp/\Delta}$ pre-plasmablasts (KO pre-PB; CD138^{-}GFP^{+}CD22^{+}) and control *Prdm1*$^{Gfp/+}$ pre-plasmablasts (pre-PB; CD138^{-}GFP^{+}CD22^{-}), which were isolated by flow cytometric sorting after 4 days of LPS stimulation. The densities of H3K27me3 at Blimp1-binding sites of repressed target genes are shown as a heat map (sorted according to increasing density in the control pre-plasmablasts). (**f**) Presence of active (H3K4me3, H3K9ac) and repressive (H3K27me3) histone marks, DHS sites, CpG islands (CGI) and Blimp1-binding sites at the *Pax5* locus in activated B cells (Act B), pre-plasmablasts (pre-PB) and plasmablasts (PB). KO, Knock-out (*Prdm1*$^{Gfp/\Delta}$).

Europe PMC Funders Author Manuscripts

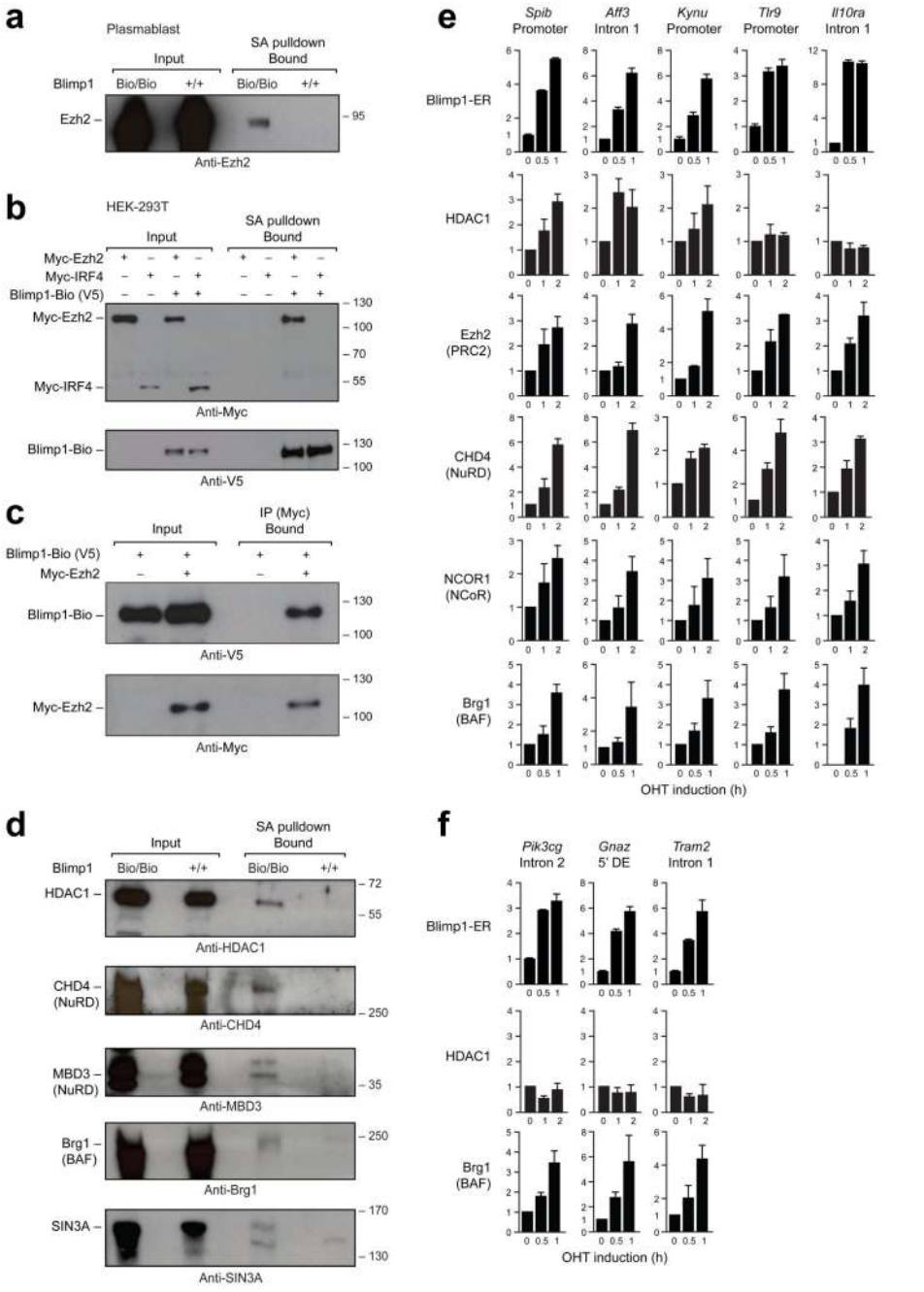

Figure 8. Blimp1-dependent recruitment of chromatin modifiers and remodelers to target genes.

(**a**) Co-precipitation of endogenous Ezh2 with Blimp1-Bio by streptavidin (SA) pulldown of extracts prepared from *Prdm1*$^{Bio/Bio}$ *Rosa26*$^{BirA/+}$ plasmablasts after 4 days of LPS stimulation. The input (1/1000) and streptavidin-bound precipitate were analyzed by immunoblotting with an anti-Ezh2 antibody. The size of marker proteins is indicated in kilodaltons to the right. (**b**,**c**) Interaction of Blimp1 with PRC2 in HEK-293T cells that were transiently transfected with the expression vectors pCMV-Blimp1-Bio-IRES-BirA and pCMV-Myc-Ezh2 or pCMV-Myc-IRF4. (**b**) The Myc-tagged Ezh2 or IRF4 proteins were

co-precipitated with the biotinylated Blimp1-Bio protein by streptavidin (SA) pulldown of nuclear extracts prepared from HEK-293T cells that were transfected with the indicated expression vectors. The input corresponds to 1/1000 of the nuclear extract used. (**c**) Blimp1-Bio was co-immunoprecipitated with the Myc-Ezh2 protein with an anti-Myc antibody. The input (1/300) and bound fraction were analyzed by immunoblotting with an anti-Myc or anti-V5 antibody to detect the Myc-tagged Ezh2 and IRF4 proteins or the V5-tagged Blimp1-Bio protein, respectively. (**d**) Co-precipitation of endogenous HDAC1, CHD4, MBD3, Brg1 or SIN3A with Blimp1-Bio by streptavidin pulldown of extracts prepared from LPS-stimulated *Prdm1*$^{Bio/Bio}$ *Rosa26*$^{BirA/+}$ plasmablasts. The input (1/1000) and streptavidin-bound precipitate were analyzed by immunoblotting with the indicated antibodies. (**e**,**f**). Rapid recruitment of histone-modifying and chromatin-remodeling complexes to repressed (**e**) and activated (**f**) Blimp1 target genes. WEHI-Blimp1-ER^{T2} B cells were treated for up to 2 h with 4-hydroxytamoxifen (OHT, 1 μM) prior to ChIP with antibodies precipitating the subunits of the indicated complexes. Input and precipitated DNA were quantified by real-time PCR with primer pairs amplifying the Blimp1-binding regions of the indicated genes and the control *Tbp* promoter. The enrichment of precipitated DNA at the target sites relative to the *Tbp* promoter was determined as described in the legend of Fig. 2g. The relative enrichment at time point 0 was set to 1. The average values and standard deviations of two (Blimp1-ER, Ezh2) or three (others) independent experiments are shown. DE, distal element.

Europe PMC Funders Author Manuscripts